ANALYSIS AND DESIGN OF A CYLINDRICAL PARABOLIC SOLAR COLLECTOR

by

Aaron Grayson Dawson, III

Thesis submitted to the Graduate Faculty of the
Virginia Polytechnic Institute and State University
in partial fulfillment of the requirements for the degree of

MASTER OF SCIENCE

in

Mechanical Engineering

APPROVED:

William C. Thomas, Chairman

Hal L. Moses

J. Robert Mahan

August 1978

Blacksburg, Virginia

ACKNOWLEDGMENTS

The author would like to thank Dr. William C. Thomas for his advice and guidance in the field of solar energy and throughout the preparation of this thesis. Thanks are also extended to faculty members and fellow students for their help while studying at Virginia Polytechnic Institute and State University. Martin Processing Company is gratefully acknowledged for the financial support of this investigation.

Finally, a special thanks is extended to his parents for their support and encouragement throughout his education and to Jayne for her patience and helpfulness during graduate school.

TABLE OF CONTENTS

	Page
ACKNOWLEDGMENTS	ii
LIST OF TABLES	iv
LIST OF FIGURES	v
NOMENCLATURE	vii
I. INTRODUCTION	1
1.1 Problem Statement	1
1.2 Weather Model Literature Review	2
1.3 Reflector Profile Literature Review	4
II. ANALYSIS	9
2.1 Weather Model	9
2.2 Cover Transmittance	14
2.3 Collector Performance Model	17
III. RESULTS AND DISCUSSION	19
IV. CONCLUSIONS AND RECOMMENDATIONS	48
REFERENCES	50
APPENDIX I - BEAM RADIATION GEOMETRY	53
APPENDIX II - THERMAL PERFORMANCE MODEL	55
VITA	64
ABSTRACT	

LIST OF TABLES

Table No.		Page
1.	Coefficients of Eq. (2.11).	13
2.	Values for Environmental and Operating Conditions	24
3.	Comparison of Collector Optimization Results.	45

LIST OF FIGURES

No.		Page
1.	Current Concentrating Collector Profiles.	6
2.	Comparison of Parabolic, Elliptic and Circular Profiles	7
3.	Cylindrical Parabolic Solar Collector Manufactured by Martin Processing Co., Inc.	20
4.	Diagram of a Cylindrical Parabolic Solar Collector.	21
5.	Distribution of Losses for the Current Concentrating Collector Design.	22
6.	Distribution of Losses for the Current Concentrating Collector Design with a Glass Cover	26
7.	Optimum Collector Orientation for a South-Facing Collector from October to March.	28
8.	Optimum Absorber Width and Location for an Inlet Temperature of 30°C	30
9.	Optimum Absorber Width and Location for an Inlet Temperature of 60°C.	31
10.	Optimum Absorber Width and Location for an Inlet Temperature of 90°C.	32
11.	Distribution of Losses for the Optimum Dimensions of a Seven-Trough Collector Using a Llumar Cover	34
12.	Optimum Number of Troughs and Absorber Widths for an Inlet Temperature of 30°C	36
13.	Optimum Number of Troughs and Absorber Widths for an Inlet Temperature of 60°C	37

14. Optimum Number of Troughs and Absorber Widths for an Inlet Temperature of 90°C 38
15. Distribution of Losses for the Optimum Dimensions of a Five-Trough Collector Using a Llumar Cover 39
16. Distribution of Losses for the Optimum Dimensions of a Five-Trough Collector Using a Glass Cover. 41
17. Distribution of Losses for a Flat-Plate Collector Using a Glass Cover 43
18. Comparison of Different Collector Designs 44
19. Collector Orientation and Beam Radiation Geometry 54
20. Ray-Trace Diagram for Off-Normal Ray Paths. 57
21. Collector Surfaces for Radiant Interchange. 60

NOMENCLATURE

Chapters I - IV

A_C - Gross collector area (m^2)

b - Distance between the bottom of the absorber and the reflector (m)

C - Ethylene glycol concentration

F - Focal length (m)

F_R - Heat removal factor

G - Fluid mass flow per unit collector area ($kg/s\text{-}m^2$)

H - Incident solar radiation (W/m^2)

I_o - Solar radiation constant (1353 W/m^2)

K_D - Ratio of scattered to total horizontal radiation

K_T - Cloudiness index

L - Cover thickness (mm)

m - Month number

n - Day number, index of refraction

Q_u - Useful energy gain from collector (W)

R - Ratio of solar radiation on a tilted surface to solar radiation on a horizontal surface

r - Ratio of hourly to daily horizontal radiation

S - Collector slope (deg)

T - Temperature (°C)

U_L - Overall loss coefficient ($W/m^2\text{-}°C$)

V - Wind velocity (m/s)

W - Absorber width (m)

X_B - Ratio of beam radiation on a tilted surface to beam radiation on a horizontal surface

X_D - Ratio of scattered radiation on a tilted surface to scattered radiation on a horizontal surface

Greek Symbols

α - Absorptance

$\hat{\delta}$ - Declination (deg)

ε - Effectiveness, emittance

ζ - "Projected" incidence angle into east-west plane normal to the collector (deg)

η - Collector thermal efficiency

η_d - Diffuse fraction

ϑ - Angle between collector normal and beam radiation (deg)

θ_Z - Zenith angle (deg)

θ_2 - Refracted angle (deg)

κ - Extinction coefficient (mm^{-1})

ρ - Reflectance

τ - Transmittance

$(\tau\alpha)$ - Transmittance-absorptance product

ϕ - Latitude (deg)

ψ - "Projected" incidence angle into north-south plane normal to the collector (deg)

ω - Hour angle (deg)

ω_s - Sunrise angle (deg)

Subscripts

a - Ambient

c - Cover

D - Diffuse

d - Diffuse

G - Ground

m - Parallel component

n - Normal component

o - Extraterrestrial

p - Absorber (plate)

r - reflector, average number of reflections

T - Total

Superscripts

h - Horizontal

t - Tilted

' - Single reflection

Additional Nomenclature for the Appendices

C_p - Specific heat (W-s/kg-°C)

C(Z) - Collector profile function (m)

D_e - Hydraulic diameter (m)

E - σT^4; Blackbody emissive power (W/m^2)

F - Configuration factor

F' - Collector efficiency factor

$\hat{G}$ - Short wave irradiation (W/m^2)

G - Long wave irradiation (W/m^2)

h - Heat transfer coefficient (W/m^2-°C)

$h_{f,i}$ - Heat transfer coefficient between the fluid and tube wall (W/m^2-°C)

h_w - Wind heat transfer coefficient, from [1] (W/m^2-°C)

$\hat{J}$ - Short wave radiosity (W/m^2)

J - Long wave radiosity (W/m^2)

K - Thermal conductivity (W/m-°C)

L - Length of collector in flow direction (m)

L_r - Average insulation thickness (m)

$Nu_{f,i}$ - Nusselt number for flow inside tubes

Pr - Prandtl number

$\dot{q}_{loss}$ - Heat loss from absorber (W/m^2)

Re - Reynolds number

S - Solar radiation heat flux (W/m^2)

T - Temperature (K)

W - Width (m)

Z_{min} - Lowest value of Z where the reflector is unshaded (m)

Z_{max} - Highest value of Z where the reflector is unshaded (m)

Greek Symbols

γ - Collector azimuth angle (deg), Beam intercept factor

γ_{sun} - Sun azimuth angle (deg)

δ_t - Absorber thickness (m)

ξ - X-axis intercept of reflected ray (m)

σ - Stefan-Boltzmann constant (W/m^2-K^4)

Subscripts

a - Aperture, ambient

B - Beam

b - Blackbody

f - Fluid

g - Gas

i - Imaginary surface

in - Inlet

L - Left

m - Mean

R - Right

I. INTRODUCTION

Flat-plate and concentrating collectors are the two main types of solar collectors. Generally, flat-plate collectors are used for relatively low temperature applications while concentrating collectors are more suitable for high temperature applications. The performance of a flat-plate collector is weakly dependent on the direction and composition of the incoming solar radiation, while the performance of a concentrating collector is strongly dependent on the nature of the incoming radiation. The directional dependence of concentrating collectors has led to a class of collectors which track the sun. The tracking systems are expensive and may be precluded by economic considerations. Clearly, stationary concentrating collectors, the subject of this investigation, could have a potentially lower manufacturing cost than the very precise tracking collectors. Stationary concentrating collectors can also have a potentially lower manufacturing cost than flat-plate collectors because they require less absorber materials and back insulation per unit aperture area than flat-plate collectors. Furthermore, concentrating collectors have a lower overall loss coefficient than a flat-plate collector as a result of concentrating the radiative flux on a smaller area. The main disadvantages of stationary concentrating collectors are the inability to concentrate diffuse radiation and the misalignment of beam radiation caused by the daily and seasonal (apparent) movement of the sun.

1.1 Problem Statement

The object of this investigation is to optimize thermally a stationary concentrating collector for a season. The optimum collector

design is one which collects the most energy at a given inlet temperature for a given season. The optimum design will depend on parameters such as latitude, type of application, weather conditions and season of operation. Since some of these parameters change during a season, a seasonal performance is more realistic than a performance evaluated at one set of environmental and operating conditions. A seasonal performance is also more helpful in designing and sizing a solar heating system for a building.

The scope of the present study includes theoretically investigating a cylindrical-parabolic collector and obtaining specific information on the distribution of losses associated with different designs. With a better understanding of the losses associated with concentrating collectors, advances can be made in improving the efficiency at reasonable manufacturing costs.

In the next section, the weather model needed for predicting the season performance of concentrating collectors is discussed. This discussion is followed by a review of the literature on concentrating solar collector reflector profiles.

1.2 Weather Model Literature Review

A seasonal performance model is needed to optimize a concentrating collector's performance. This model must have, as a minimum, weather input parameters for specific locations. Solar radiation, ambient temperature, and wind speed are the major parameters affecting collector performance. Most solar radiation data are in the form of daily total radiation on a horizontal surface [1-6]. This form of insolation data

can be used to evaluate solar collector performance by constructing "typical" daily distributions of beam and scattered radiation. Hourly average values are generally sufficiently accurate for the purpose of investigating collector performance.

Liu and Jordan [7] developed a procedure for converting average daily total radiation on a horizontal surface into hourly beam and hourly scattered radiation in the plane of an arbitrarily-oriented collector. Their model is the most commonly used model in flat-plate and concentrating collector performance analyses. Their method [7], without any major changes, has been in use for eighteen years. Norris [8] compared Liu and Jordan's results to actual measurements in the plane of collector and found remarkably good agreement (within seven percent).

Other authors [8-14] have proposed alternate methods for segments of Liu and Jordan's basic procedure. References 8,9,12,13 and 14 are based on empirical formulations and require either additional weather information or are restricted to certain latitudes and locations. Norris [9] and Reddy [13] require the type of cloud cover be specified. Alternately, Reddy [14] requires the mean humidity, number of rainy days per month, and fraction of bright sunshine per day be specified. Iqbal [10] also requires specifying the fraction of bright sunshine per day. The modifications proposed in references 8,9,10,12,13 and 14 were considered for the present study but were not used because of the lack of generality and because the additional weather data is not generally available. Heywood [11] suggested using solar declination periods instead of months. Although his approach could be an improvement, most available

weather data are reported in terms of monthly averages.

There are three main methods available to determine the seasonal performance of a collector using monthly average weather data. One method is the "f-chart" method designed by Beckman, Klein and Duffie [3]. Their method applies to flat-plate collectors only and is therefore not pertinent to this study. A second method [5] is one which uses "utilizability curves" and calculated values for the primary collector performance parameters: $(\tau\alpha)$, F_R, and U_L. This method is used primarily for flat-plate collectors, but through some modifications can be used for concentrating collectors. The third method is to use energy balance equations from Duffie and Beckman [1], and ray tracing techniques from Thomas [15]. The second and third methods are similar but the third method is more adaptable to parameter studies. The third method was experimentally verified for normal radiation by Smith [16]. For the reasons previously noted, a weather model based on Liu and Jordan [7] along with a collector performance model based on Duffie and Beckman [1] and Thomas [15] are used to optimize the design with respect to thermal performance of a cylindrical concentrating collector.

1.3 Reflector Profile Literature Review

There is still a question as to the best shape for a reflector in a fixed cylindrical concentrating collector. The optimum fixed cylindrical concentrating collector would direct all off-normal beam radiation, resulting from daily and seasonal movements of the sun, to the absorber and still maintain a high concentration ratio. Meinel [7] examines several different profiles that attempt to accomplish these requirements.

One of the most popular profiles currently is the Winston compound parabolic reflector [18,19,20]. A characteristic of this profile is a high concentration ratio for a large acceptance angle. The Winston profile consists of two symmetrical half-parabolic cylinders with foci placed on each other and the "tops" parallel to the normal axis as shown in Fig. 1a. A variation of the Winston design is one which widens the aperture area to achieve a higher concentration ratio, but at the expense of an extra reflection. This shape is discussed by Meinel [17] and Rabl, et al. [21] and shown in Fig. 1b. Present reflectivities of approximately 80 percent practically preclude the use of this profile due to the loss from the extra reflection.

The high cost of manufacturing compound parabolic reflectors has lead to a class of less efficient, but easier to manufacture, reflectors. These include the simple V-groove reflectors analyzed by Weibelt [22], the composite trapezoidal groove reflectors investigated by Villanneva and Trong [23], and segments of circular profile developed by Shapiro [24]. These shapes are shown, respectively, in Figs. 1c-1e.

The classical shapes are the parabolic, elliptical and circular profiles shown in Fig. 2. The differences in profile are slight, but the performance can differ markedly for off-normal beam radiation angles. Smith [16] investigated a cylindrical-elliptical collector manufactured by Martin Processing Company, Inc. An earlier manufacturing process of cutting the trough with an inclined circular saw produced the elliptical profile. Recent manufacturing changes have resulted in a parabolic reflector profile. Therefore, the scope of this investigation deals

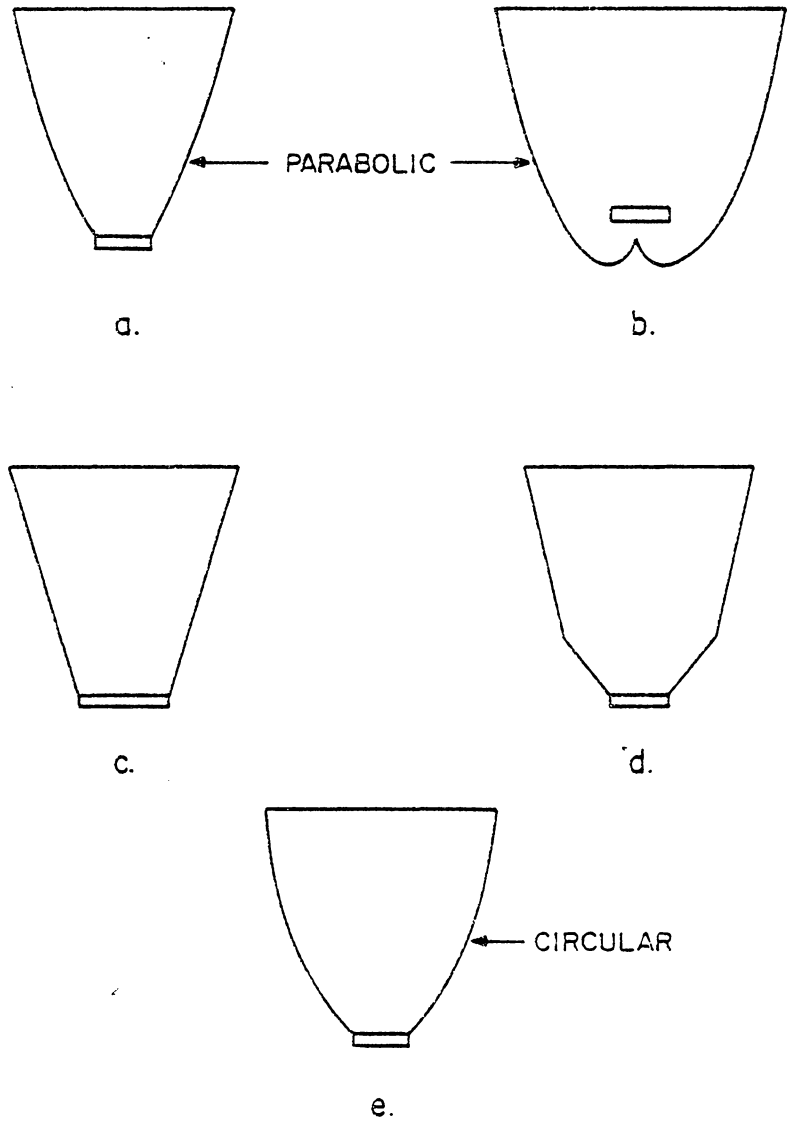

Figure 1. Current Concentrating Collector Profiles: (a) Compound parabolic; (b) Cusplike compound parabolic; (c) V-groove; (d) Composite trapezoid; and (e) Segments of circular profile.

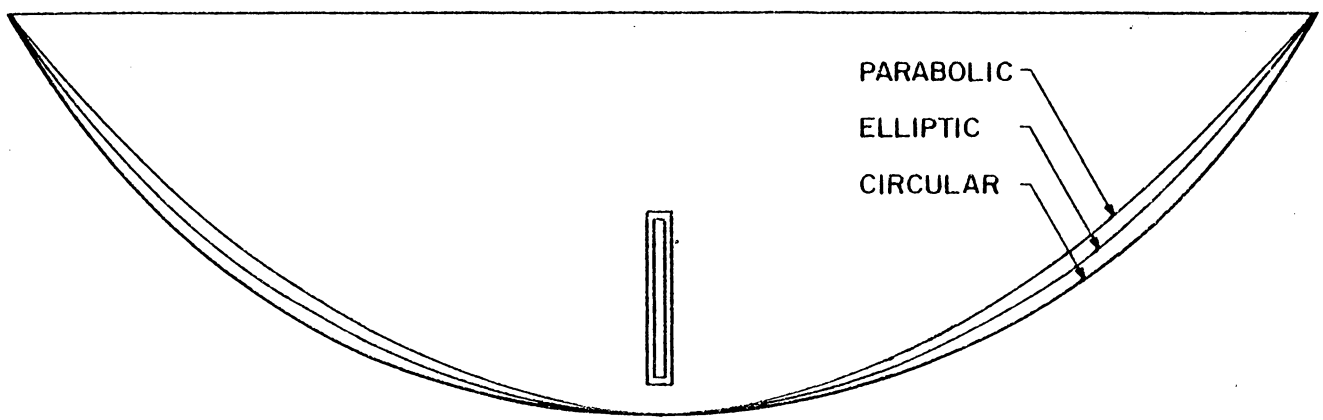

Figure 2. Comparison of Parabolic, Elliptic and Circular Profiles

primarily with parabolic profiles and an optimization of the present design of the Martin Processing Company's concentrating collector.

The theory needed to optimize the present concentrating collector design is developed in the next chapter. A weather model supplies solar radiation data, angles of beam radiation, ambient temperatures and wind speeds to a collector performance model. The collector performance model is an extension of the present state-of-the-art collector theory and includes ray-tracing techniques, energy balances on collector components and an accurate model of the cover transmittance. The collector performance model gives values for the total energy collected in a season in order to determine the optimum design. Clearly, economics are important in determining the optimum design but are not specifically included in the present investigation.

II. ANALYSIS

2.1 Weather Model

A weather model is needed to determine the average collector output for a season. Several methods are used to obtain solar radiation availability. One method is to obtain hourly data from a nearby weather station and project future performance based on data from one or several seasons. Hourly data are not available for most locations. A one-year sample may not be representative of future weather conditions. Also, predicting collector performance hourly for the season requires an excessive amount of computer time. A second method is to use the average solar radiation available for a month, and, from this value, predict the monthly performance. Because the performance of a solar collector is not linear with solar radiation, this method could lead to large uncertainties. A third method is to use monthly averages of total radiation on a horizontal surface, H_T^h, and convert this value to hourly radiation in the plane of the collector. As of 1972, 86 weather stations record H_T^h. Since these values are long-term averages, future predictions are more reliable. Liu and Jordan [7], employ a procedure for manipulating H_T^h data into hourly beam and scattered radiation in the plane of the collector. This procedure has a minimum of inputs, is fairly easy to implement in equation form, and has been verified by measurements. For these reasons, the procedure by Liu and Jordan is used as the basis for the weather model.

The input parameters for this model are H_T^h data, latitude, azimuth angle, and collector slope. All data is based on the mid-day of each month (day 15 or 16). The day number associated for that month is

$$n = 15 + 30.24\ (m-1) \quad , \tag{2.1}$$

where m is the number of the month. The equations for the declination, sunrise angle, and the daily extraterrestrial solar radiation are, respectively,

$$\delta = 23.45\ \sin[360(284 + n)/365], \tag{2.2}$$

$$\omega_S = \text{arc cos}[-\tan\phi\tan\delta], \tag{2.3}$$

and

$$H_o = 37\ 210[1 + 0.033\ \cos(\frac{360n}{365})][\cos\phi\cos\delta\cos\omega_S + \pi/180\ \omega_S\ \sin\phi\sin\delta]. \tag{2.4}$$

In order to determine the percentage of H_T^h that is scattered radiation, a cloudiness index, K_T, is introduced. The cloudiness index is the fraction of extraterrestrial radiation that is transmitted through the atmosphere. A high K_T indicates a locality with clear weather while a low K_T indicates a cloudy region. A relationship between the ratio of H_D^h to H_T^h, K_D, and the cloudiness index is obtained from fitting a curve to the data in [7].

$$K_D = H_D^h/H_T^h = 1.444 - 4.410\ K_T + 6.300\ K_T^2 - 3.594\ K_T^3 \ . \tag{2.5}$$

Once the daily total and daily scattered radiation have been determined, the hourly radiation can be obtained from correlations in references 25 and 26. The theoretical ratio for hourly to daily horizontal radiation can be obtained by integrating the extra-terrestrial radiation on a horizontal surface for one hour and one day. The ratio is

$$r_o = \frac{\int_{\omega_1}^{\omega_2} I_o \cos\theta_Z d\omega}{2\int_{\omega_s}^{0} I_o \cos\theta_Z d\omega} , \qquad (2.6)$$

or

$$r_o = \frac{\int_{\omega_1}^{\omega_2} I_o(\sin\delta\sin\phi+\cos\delta\cos\phi\cos\omega)d\omega}{2\int_{\omega_s}^{0} I_o(\sin\delta\sin\phi+\cos\delta\cos\phi\cos\omega)d\omega} \qquad (2.7)$$

After integration and simplification, Eq. (2.7) yields

$$r_o = \frac{[\sin\omega_1-\sin\omega_2 - (\omega_1-\omega_2)\cos\omega_s]}{2[\sin\omega_s-\omega_s\cos\omega_s]} . \qquad (2.8)$$

For the hourly values, let ω correspond to the middle of a given hour. Then

$$r_o = \frac{\sin(\omega+\frac{\pi}{24})-\sin(\omega-\frac{\pi}{24})-\frac{\pi}{12}\cos\omega_s}{2[\sin\omega_s - \omega_s\cos\omega_s]} , \qquad (2.9)$$

or, after using a trigonometric identity and some simplification,

$$r_o = \frac{\pi}{24}\left[\frac{0.997\cos\omega-\cos\omega_s}{\sin\omega_s-\omega_s\cos\omega_s}\right] . \qquad (2.10)$$

The data in references 25 and 26 agree well with the theoretical ratio for scattered radiation, while the total radiation data do not. This discrepancy could be a result of the difference in attenuation of beam radiation in the atmosphere at different hour angles. Curve fits to the hourly total data in references 26 and 26 yield

$$r_{T,\omega} = a_{0,\omega} + a_{1,\omega}\,\omega_S + a_{2,\omega}\,\omega_S^2 \quad , \tag{2.11}$$

for $\omega = \pm\frac{\pi}{12}, \pm\frac{\pi}{4}, \pm\frac{5\pi}{12}, \pm\frac{7\pi}{12}, \pm\frac{3\pi}{4}, \pm\frac{11\pi}{12}, \pm\frac{13\pi}{12}$.

The coefficients in Eq. (2.11) are listed in Table 1.

Since most solar collectors are operated at some angle of tilt from the horizontal, the hourly total and hourly scattered radiation values for a horizontal surface must be converted into radiation on a tilted surface. The form of radiation incident on the tilted collector is composed of beam radiation from the sun, scattered radiation from the sky, and reflected radiation from the ground. The conversion ratio for the beam component is

$$X_B = \frac{\cos\theta}{\cos\theta_Z} \quad . \tag{2.12}$$

Assuming the scattered radiation from the sky is diffuse, the tilted collector receives a fraction of the sky radiation equal to $\frac{1}{2}(1+\cos S)$. The collector also receives a fraction of the total radiation reflected off the ground equal to $\frac{1}{2}(1-\cos S)$. Thus the conversion ratio for the scattered (diffuse) component is

$$X_D = \tfrac{1}{2}(1 + \cos S) + \tfrac{1}{2}(1 - \cos S)\rho_G/K_D \quad . \tag{2.13}$$

Table 1. COEFFICIENTS OF EQ. (2.11)

ω	$\pm \frac{\pi}{12}$	$\pm \frac{\pi}{4}$	$\pm \frac{5\pi}{12}$	$\pm \frac{7\pi}{12}$	$\pm \frac{3\pi}{4}$	$\pm \frac{11\pi}{12}$	$\pm \frac{13\pi}{12}$
a_0	0.3746	0.2720	0.0602	-0.1729	-0.2481	-0.0611	-7.429×10^{-3}
a_1	-3.734×10^{-3}	-2.178×10^{-3}	1.244×10^{-3}	4.907×10^{-3}	5.216×10^{-3}	7.570×10^{-4}	-2.986×10^{-4}
a_2	1.276×10^{-5}	6.407×10^{-6}	-8.197×10^{-6}	-2.370×10^{-5}	-2.233×10^{-5}	6.356×10^{-7}	4.257×10^{-6}

Finally, the hourly total radiation incident on the plane of the collector is

$$H_T^t = (H_T^h - H_D^h) X_B + H_D^h X_D \quad , \tag{2.14}$$

with a diffuse fraction equal to

$$\eta_d = \frac{H_D^h X_D}{H_T^t} \quad . \tag{2.15}$$

Equations for the incidence angle, and other pertinent angles relative to the collector are given in Appendix I.

Other environmental parameters affecting collector performance are ambient temperature and wind speed. The ambient temperature used should be the average daytime temperature, and the wind speed should also be the daytime average. These average quantities can be obtained from many airports and weather stations. Altitude, humidity, and atmospheric dust are environmental parameters which have a minor effect on collector performance but were neglected.

2.2 Cover Transmittance

During the course of a day, a non-tracking solar collector will receive radiation over a large range of incidence angles. To accurately model the cover transmittance throughout this range of incidence angles, a theoretical model more complete than a transmittance evaluated at an average incidence angle is needed. A collector having one cover is analyzed first.

The reflection of nonpolarized radiation is found for each component of radiation by the following equations derived by Fresnel,

$$\rho_m' = \sin^2(\theta_2-\theta)/\sin^2(\theta_2+\theta), \tag{2.16a}$$

and

$$\rho_n' = \tan^2(\theta_2-\theta)/\tan^2(\theta_2+\theta), \tag{2.16b}$$

where θ_2 is found from Snell's law for a transparent media with $n>>\kappa$,

$$\theta_2 = \text{arc sin } [(\sin\theta)/n]. \tag{2.17}$$

The absorption of radiation in the cover is found by integrating Bouger's Law and gives

$$\tau_a = \exp(-\kappa L/\cos\theta_2). \tag{2.18}$$

The reflectances for one cover including multiple reflections within the cover material are

$$\rho_m = \rho_m' \, [1+\tau_a^2(1-2\rho_m')]/[1-(\tau_a\rho_m')^2], \tag{2.19a}$$

and

$$\rho_n = \rho_n' \, [1+\tau_a^2(1-2\rho_n')]/[1-(\tau_a\rho_n')^2]. \tag{2.19b}$$

The total reflectance is found by averaging the two components of reflectance, giving

$$\rho = (\rho_m+\rho_n)/2 \ . \tag{2.20}$$

The transmittances can be found in a manner similar to the reflectances and are

$$\tau_m = \tau_a[1-\rho_m]^2/[1-(\tau_a\rho_m)^2], \tag{2.21a}$$

$$\tau_n = \tau_a[1-\rho_n]^2/[1-(\tau_a\rho_n)^2], \tag{2.21b}$$

and

$$\tau = (\tau_m + \tau_n)/2 \quad . \tag{2.22}$$

For cover systems with two or more covers, Eqs. (2.16)-(2.22) are applied to each cover, and combined in the following manner to obtain the overall reflectance and transmittance. The top two covers are combined to yield

$$\rho_{1,2} = \rho_1 + \rho_2\ \tau_1^2/[1-\rho_1\rho_2] \ , \tag{2.23}$$

and

$$\tau_{1,2} = \tau_1\ \tau_2/[1-\rho_1\rho_2] \ . \tag{2.24}$$

The top two covers are now treated as one compound cover, and combined with the third cover as follows,

$$\rho_c = \rho_{1-2,3} = \rho_{1,2} + \rho_3\ \tau_{1,2}/[1-\rho_{1,2}\ \rho_3] \ , \tag{2.25}$$

and

$$\tau_c = \tau_{1-2,3} = \tau_{1,2}\ \tau_3/[1-\rho_{1,2}\ \rho_3] \quad . \tag{2.26}$$

Solar collectors with more than three covers are uncommon, but could be analyzed in a similar manner. If the scattered fraction of radiation is assumed diffuse, the diffuse transmittance can be

calculated from Ramsey, et al. [27] as

$$\tau_d = \int_0^{\pi/2} \tau_c(\theta) \sin(2\theta)\, d\theta \quad . \tag{2.27}$$

Equation (2.27) must be integrated by numerical means as a result of the complicated function $\tau_c(\theta)$. The transmittance-absorptance product can now be calculated as follows,

$$(\tau\alpha) = \alpha_p[(1-\eta_d)\tau_c + \eta_d\tau_d]/[1-(1-\alpha_p)\rho_{c,60}], \tag{2.28}$$

where $\rho_{c,60}$ is the diffuse reflectance of the cover system, which is approximately the cover reflectance at an incidence angle of 60 degrees.

2.3 Collector Performance Model

The collector performance model used to thermally analyze different collector designs was developed by Thomas [15] and modified by the author for parabolic profiles. The performance model is based on state-of-the-art collector theory [1] consisting of energy balances on the collector components and ray-tracing techniques to determine the radiative flux on the absorber. The environmental conditions, operating conditions, collector dimensions, heat transfer properties, and optical properties must be specified to calculate the useful energy collected. The thermal analysis, ray-tracing logic, and equations used in the collector performance model are in Appendix II.

Smith [16] verified the theoretical model used in this

investigation experimentally with collector efficiency tests and found the model adequate for use as a design assistance tool. The theoretical efficiency intercept was within 2.5 percent of the experimental efficiency intercept and the theoretical stagnation temperature was within 10°C of the experimental stagnation temperature. This model, with environmental conditions supplied by the weather routine, are used in a parameter study of the Martin Processing Company's concentrating collector in the next chapter.

III. RESULTS AND DISCUSSION

The cylindrical-parabolic concentrating collector to be optimized is shown in Fig. 3. The collector contains seven identical parabolic troughs with flattened copper tubes as the absorbers. The absorber has a selective surface with an estimated absorptance and emittance of 0.93 and approximately 0.20, respectively. The reflectors are constructed from polished aluminum sheets formed into shape by parabolic supporting ribs along the length of the cylinder. The cover material, Llumar*, is a weatherable polyester film. Fiberglass insulation is added between the reflectors and the back cover to reduce back conduction losses. Fig. 4 shows a cross-section of the collector with the dimensions and nomenclature as used in the parameter study.

Fig. 5 was constructed to compare the distribution of losses for the present collector design. Each of these losses is described below:

(a) Cover losses result from radiation absorbed in and reflected from the cover, i.e., $\tau_c < 1$ and $\rho_c > 0$.

(b) Absorptance losses result from an imperfect absorber, i.e., $\alpha_p \neq 1$.

(c) Beam intercept losses result from beam radiation which leaves the reflector and does not intercept the absorber. The loss can be caused by a misaligned absorber, an absorber of insufficient width, or the reflecting profile.

(d) Reflector losses result from an imperfect reflector, i.e., $\rho_r \neq 1$.

*Registered trade name, Martin Processing Company.

Fig. 3. Cylindrical Parabolic Solar Collector Manufactured by Martin Processing Co., Inc.

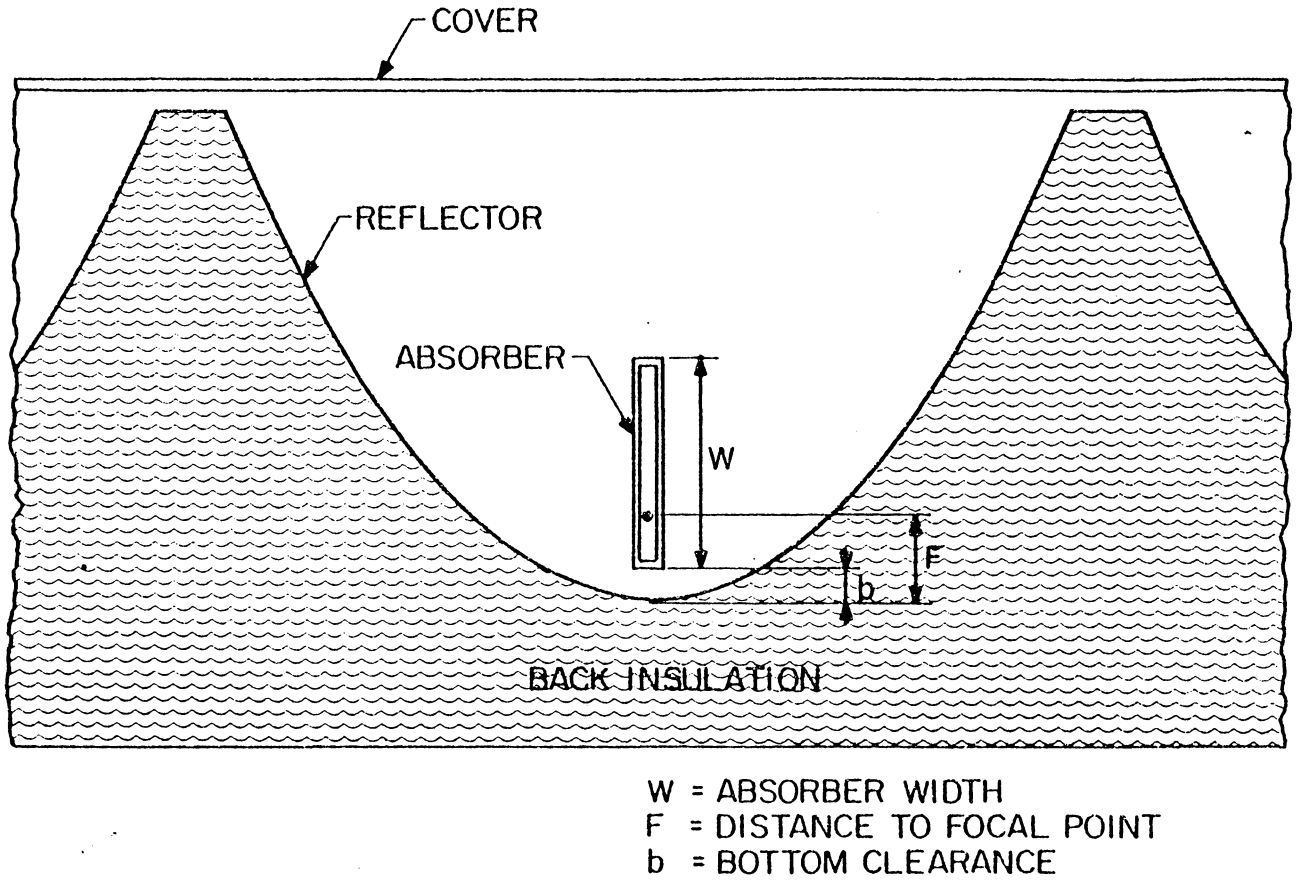

Figure 4. Diagram of a Cylindrical Parabolic Solar Collector

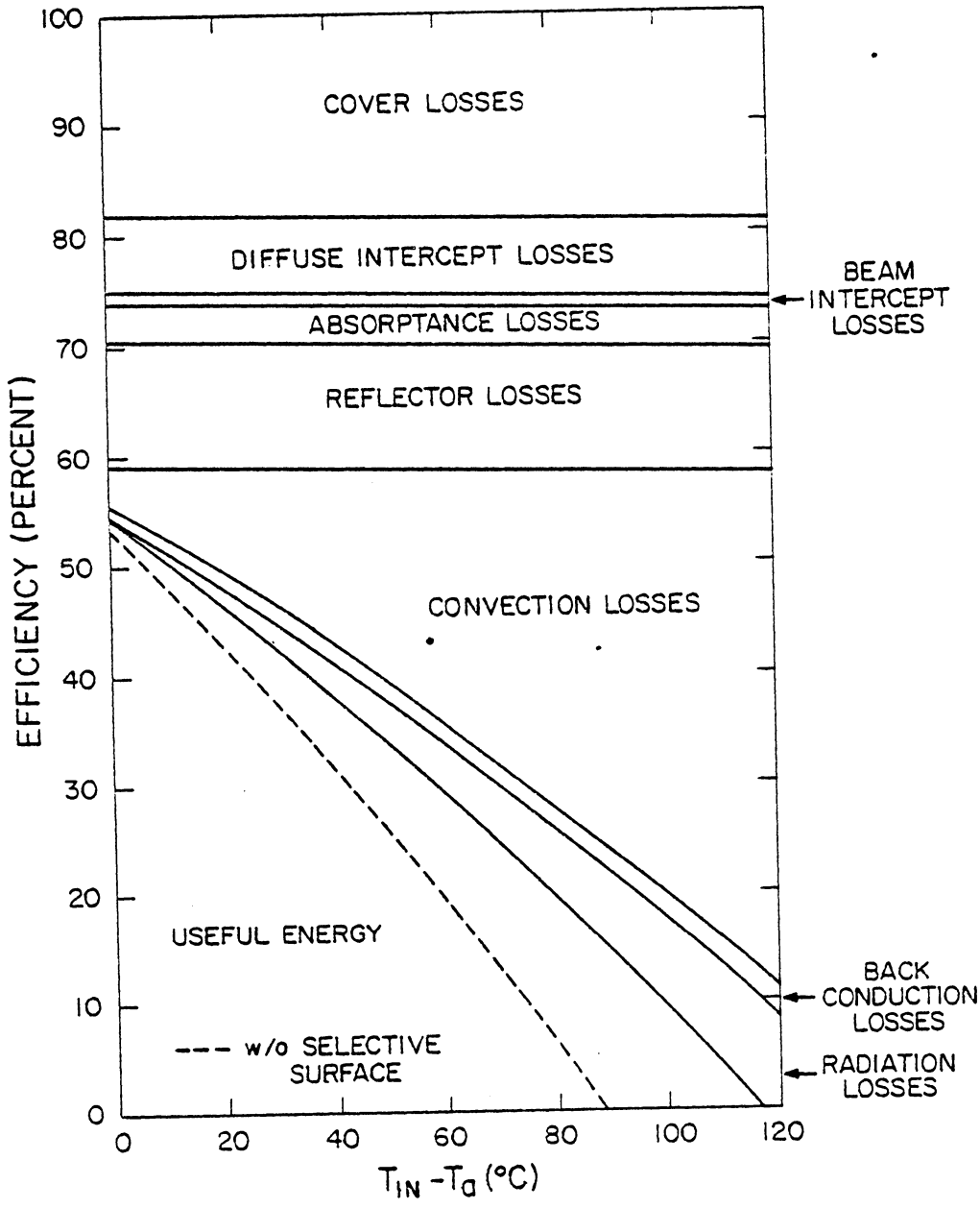

Figure 5. Distribution of Losses for the Current Concentrating Collector Design

(e) Convection losses result from heat lost from the absorber to the surrounding gas by natural convection.

(f) Back conduction losses result from heat lost from the back of the collector.

(g) Radiation losses result from (long wave) radiation emitted from the absorber to the ambient and sky.

The distribution of collector losses was obtained by starting with components having perfect properties and individually considering actual components. (The calculation procedure precluded setting the convection losses exactly equal to zero, which caused a slight slope in the optical loss curves.) The dashed curve represents the collector's performance without a selective surface. Environmental and operating conditions used to construct Fig. 5 are listed in Table 2. These conditions are normal testing conditions, which are somewhat better than seasonal averages. The distribution of losses, however, is not very sensitive to environmental conditions.

Fig. 5 shows that the main losses are a result of convection, reflection, and cover transmittance. The "optical" efficiency, or efficiency when the mean absorber temperature is equal to the ambient temperature, is 59 percent. This efficiency corresponds to $(\tau\alpha)$ in flat-plate collectors and is generally about 85 percent when high quality glass is used for the cover.

Of the three main losses, the cover and reflector losses are limited by the materials used. Using glass for the cover and a thin layer of silver for the reflector could reduce these losses, but the added

Table 2. VALUES FOR ENVIRONMENTAL AND OPERATING CONDITIONS

T_a = 15°C	H_T^t = 800 W/m^2	S = 52 deg
η_d = 0.15	G = 0.02 kg/(s•m^2)	ψ = 7.5 deg
V = 3.1 m/s	C = 0.5 ethylene glycol	ζ = 0 deg

cost would have to be considered. Fig. 6, similar to Fig. 5, shows the performance when the plastic cover is replaced by a glass cover. The glass has an index of refraction equal to 1.518 and an extinction coefficient equal to 0.11 mm^{-1}. The normal transmittance of the glass is 0.89 and the long wave transmittance is 0.02. The glass cover adds four percentage points to the efficiency at the lowest inlet temperature and five percentage points to the efficiency at the highest inlet temperature. (The efficiency is one percentage point better for high inlet temperatures as a result of the lower long wave transmittance of glass.) The added cost of glass would be more nearly cost beneficial at higher rather than lower inlet temperatures.

The convection losses can be reduced by adding a convection suppressor or by decreasing the area of the absorber. A convection suppressor could be an additional cover or a highly transparent tube over the absorber. Both suppressors would increase the cover losses. The economic feasibility would depend on the operating temperature as well as the transmissivity of the suppressors. Decreasing the absorber size would reduce the convection losses and, to a small degree, radiation losses but would increase the beam intercept losses. At higher inlet temperatures, a tradeoff between decreasing the convection losses while increasing the beam intercept losses may give an overall increase in the performance of the collector.

The optimization of the present collector design involves a parametric study on the dimensions of the collector for three different temperature ranges. These temperatures, which are 30°C, 60°C and 90° C,

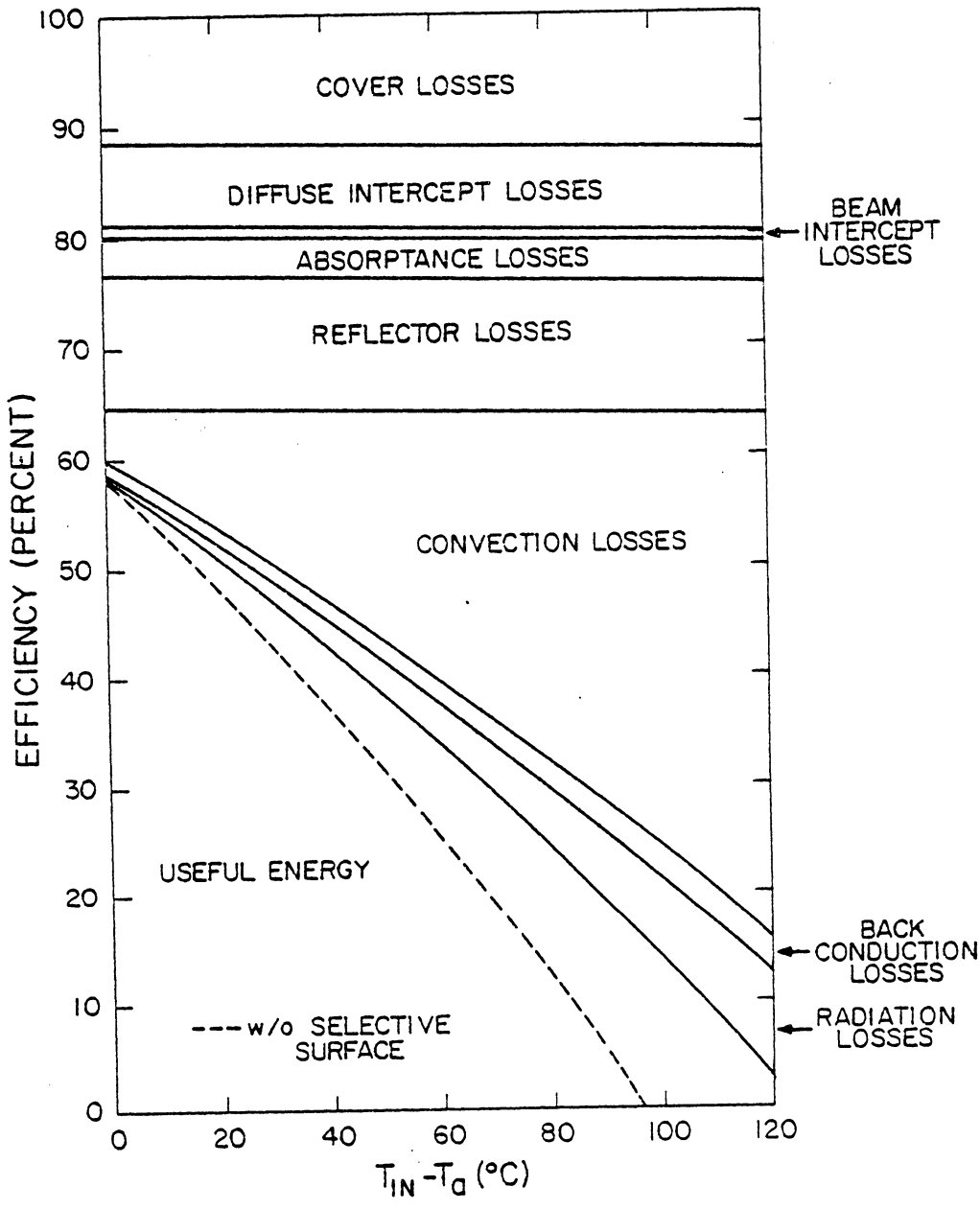

Figure 6. Distribution of Losses for the Current Concentrating Collector Design with a Glass Cover

correspond to operational temperatures for domestic hot water, space heating, and process heat, respectively. It is assumed in the optimization study that all of the solar energy collected can be used. This assumption is fully valid for solar energy systems supplying about one-half or less of the total energy requirements. The weather data used is from Blacksburg, Virginia, and is considered to be representative of the middle eastern coast of the United States. Domestic hot water and process heat are used year-round while space heating is required only for the winter months. However, to save considerable computer time, the optimization was performed over a symmetric, with respect to the declination, six-month period, starting in October and ending in March.

The optimum orientation of the present collector design must be obtained for the season to minimize the off-normal incidence angles with respect to the normal of the collector. Fig. 7 shows a plot of the effectiveness as a function of the collector slope for a south-facing collector. The effectiveness is defined as the ratio of the useful energy per unit area collected to the total horizontal insolation. Effectiveness is used instead of the efficiency because a mis-oriented collector can have a high efficiency, but collect little useful energy. The effectiveness and efficiency are related by the following equation,

$$\varepsilon = \frac{Q_u/A_C}{H_T^h} = \frac{Q_u/A_C}{H_T^t} R = \eta R. \qquad (3.1)$$

Note that the effectiveness can be greater than one.

Fig. 7 applies to arbitrary locations as a result of subtracting the latitude from the collector slope. This reasoning can be deduced by

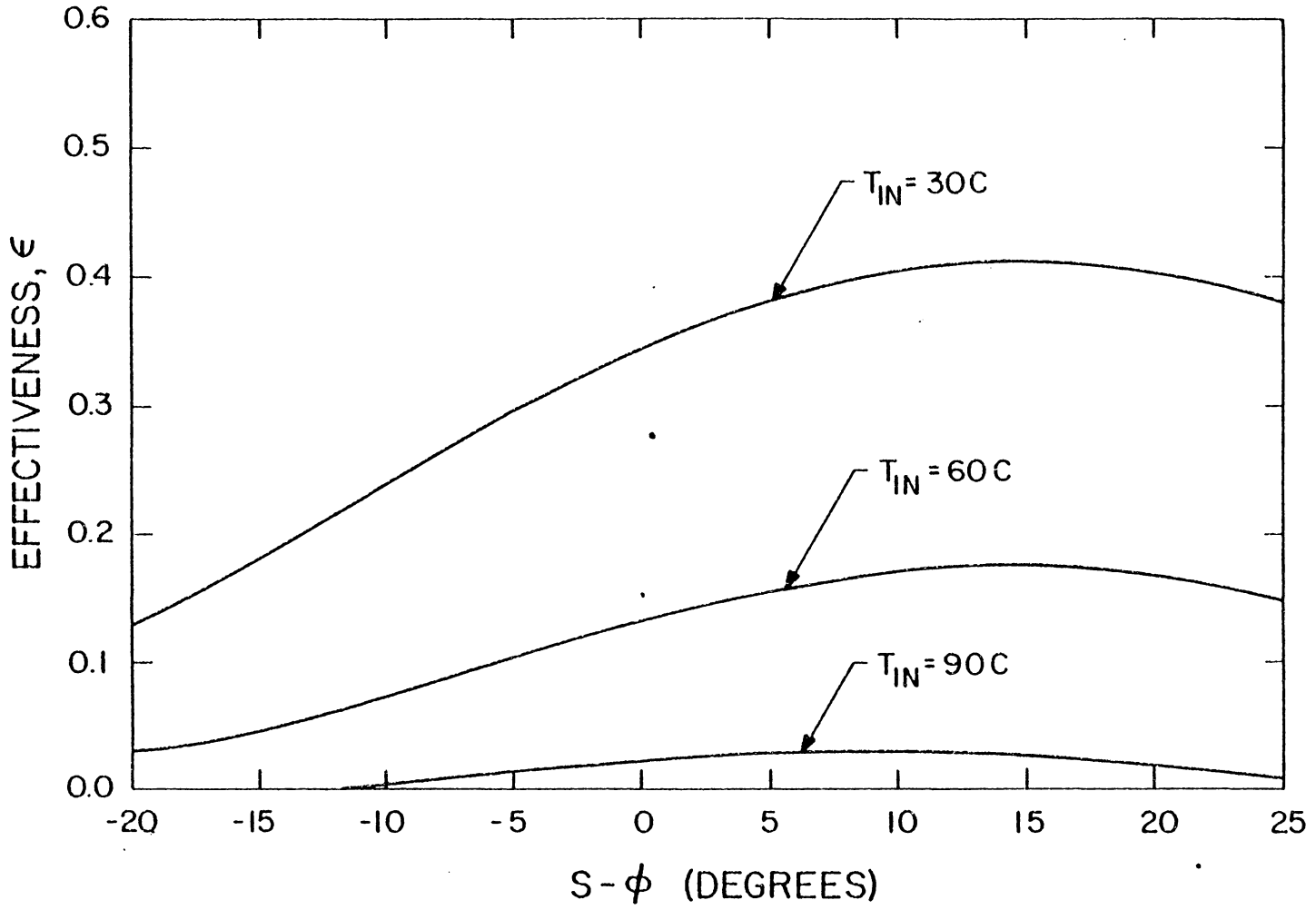

Figure 7. Optimum Collector Orientation for a South-Facing Collector From October to March

using the incident angle equation in Appendix I for a south-facing collector at solar noon, which gives

$$\cos\theta = \sin\delta \sin\theta \cos S - \sin\delta \cos\theta \sin S + \cos\delta \cos\theta \cos S + \cos\delta \sin\theta \sin S. \quad (3.2)$$

Using a trigonometric identity and further simplification yields

$$\theta = \delta + S - \phi. \quad (3.3)$$

The maximum energy available during a day for a fixed collector occurs when θ is zero in Eq. (3.3). Therefore, the optimum collector slope for any given day is the latitude minus the declination. Since the latitude is constant throughout the season, it can be subtracted from the collector slope and make the result independent of location. The seasonal energy collected, however, is a function of the insolation, declination, latitude and collector slope for the season and cannot be expressed as a simple relation. The optimum heating season collector slope from Fig. 7 is the latitude plus 15 degrees.

The width and position of the absorber can have a large influence on the performance of a concentrating collector. A balance must be considered between the heat loss from the absorber and the fraction of radiation intercepted by the absorber. Figs. 8-10 show the effect of absorber width and position above the reflector on collector effectiveness. The optimum widths for inlet temperatures of 30°C, 60°C and 90°C are 30 mm, 25 mm and 10 mm, respectively. The corresponding bottom clearances for inlet temperatures of 30°C, 60°C and 90°C are 0, 0 and 7.5 mm, respectively. Figs. 8-10 also show that for any absorber width the

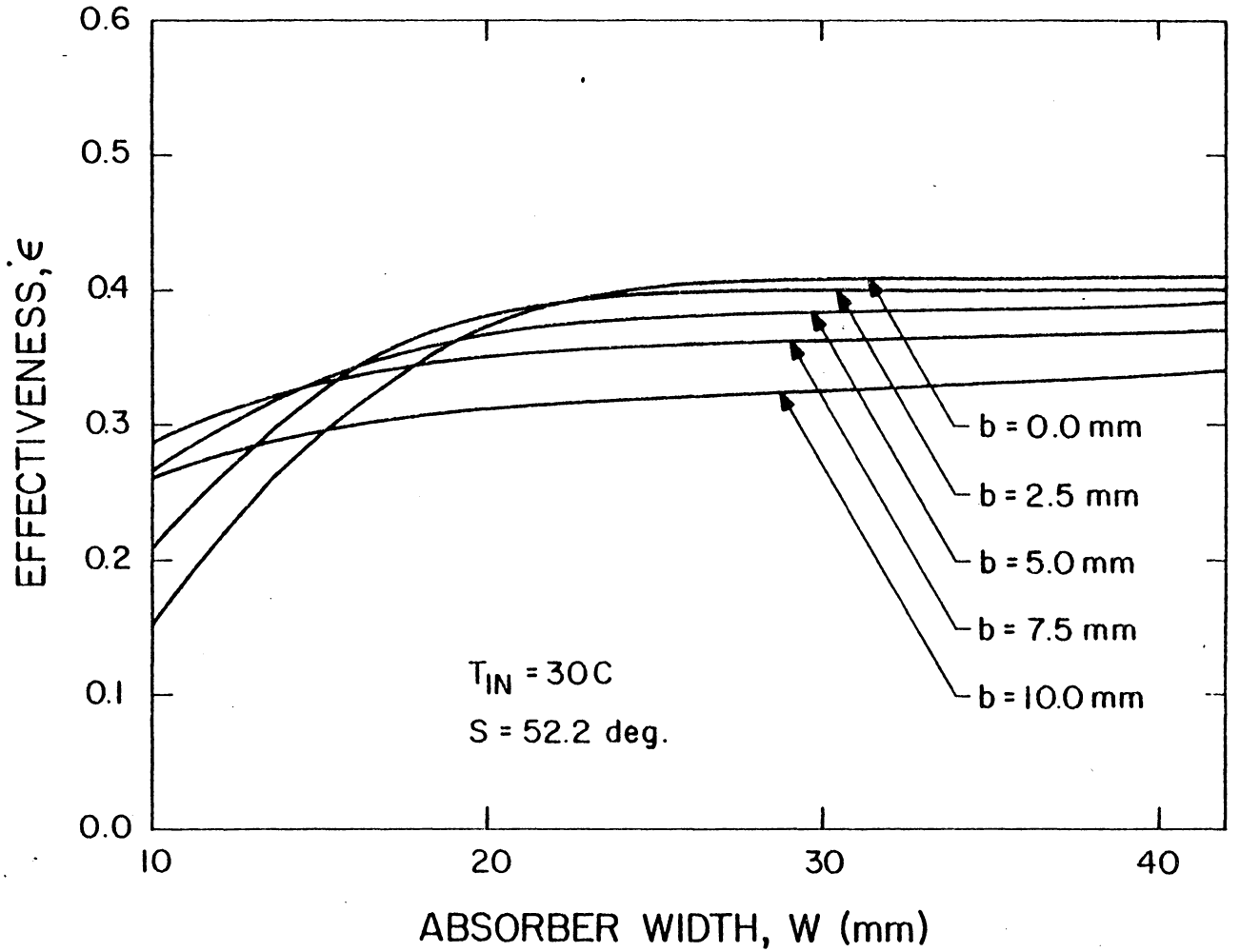

Figure 8. Optimum Absorber Width and Location for an Inlet Temperature of 30°C

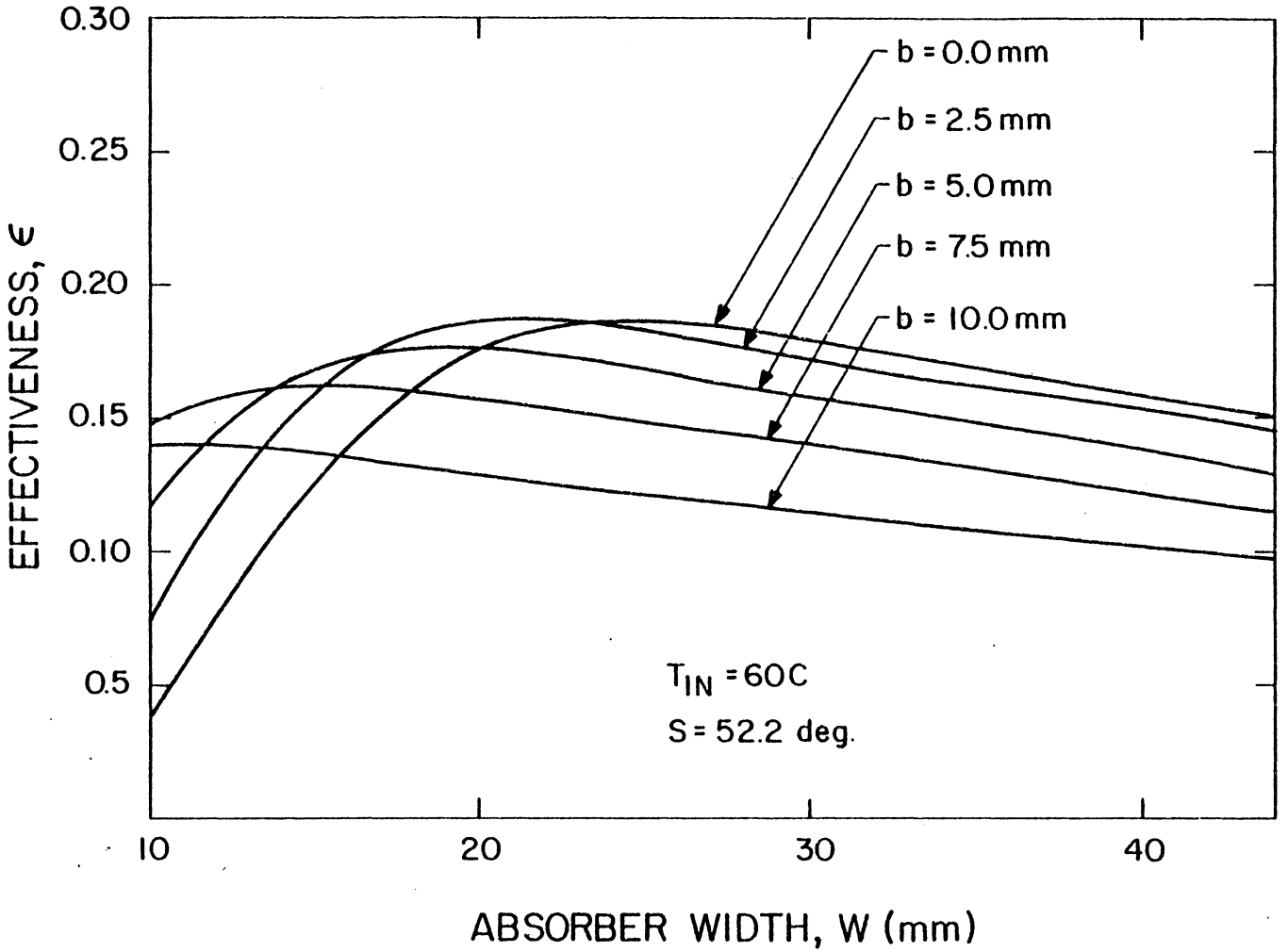

Figure 9. Optimum Absorber Width and Location for an Inlet Temperature of 60°C

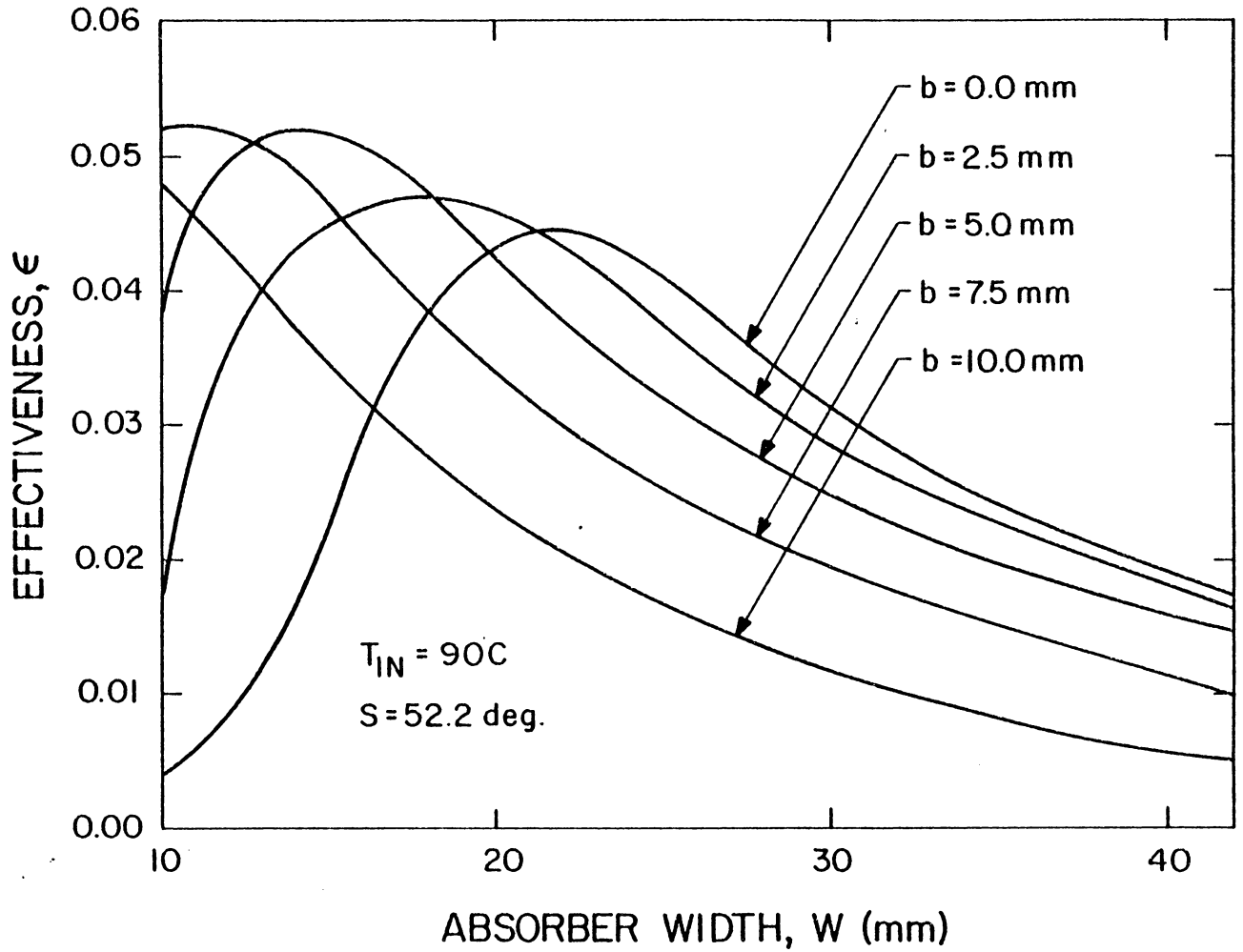

Figure 10. Optimum Absorber Width and Location for an Inlet Temperature of 90°C

optimum bottom clearance is

$$b = F - W/2 \quad \text{for } W \leq 2F,$$

and

$$b = 0.0 \quad \text{for } W > 2F. \tag{3.4}$$

Equation (3.4) shows that the absorber should be centered at the focal point or resting on the reflector. In practice, a small space should be left between the absorber and reflector to minimize conduction losses. Also, the unusually small absorber width, calculated for an inlet temperature of 90°C may cause positioning and strength problems during manufacturing and high pressure drops during operation.

Fig. 11 shows the distribution of losses for a collector with an absorber width of 25 mm and no bottom clearance. The 7 mm decrease in absorber width, compared with the existing design, causes the "optical" losses to increase by two percentage points. The overall loss coefficient or slope of the curve in Fig. 11 is decreased slightly, causing an intersection of the curves in Figs. 5 and 11 at a temperature difference of approximately 30°C. Therefore, an absorber width of 25 mm should be used instead of the existing absorber width of 32 mm for temperature differences greater than 30°C.

The collector is now essentially optimized without major changes in materials and structure. Since the cost of the collector is proportional to the number of troughs used, the effect of reducing the number of troughs on the collector effectiveness is considered. Increasing the thickness of the collector does not increase the potentially available energy, but does increase the material costs. Therefore, for a constant trough depth, the aperture width should be increased resulting in fewer

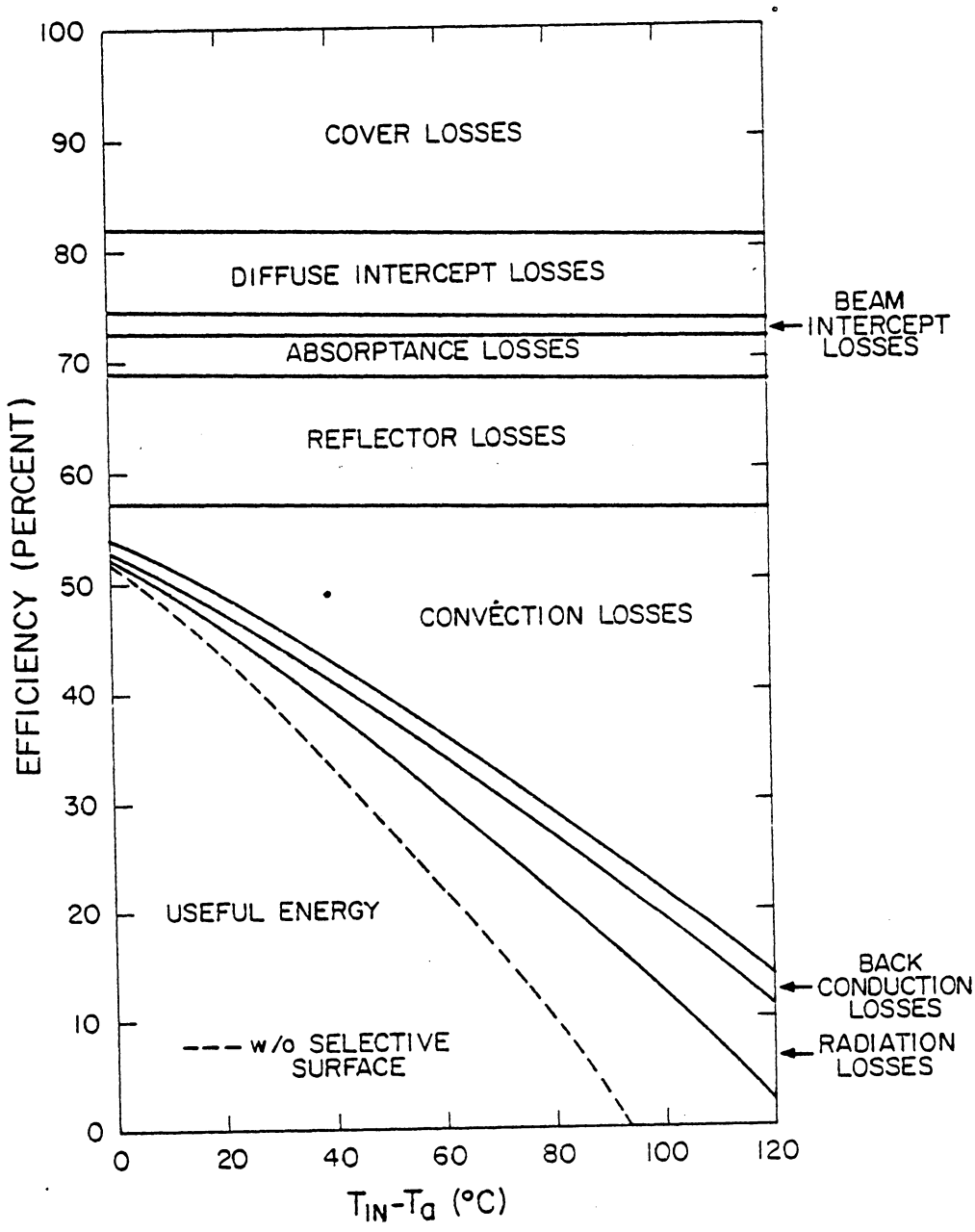

Figure 11. Distribution of Losses for the Optimum Dimensions of a Seven-Trough Collector Using a Llumar Cover

troughs. Increasing the aperture width increases the focal length and sensitivity of the concentrator to the angle ψ. A parameter study of absorber widths is, therefore, necessary. Figs. 12-14 show curves for the present collector with seven troughs and collectors with six, five and four troughs. A bottom clearance calculated from Eq. (3.4) is used in these curves. The curves in Figs. 12-14 show only a five percent loss of useful energy with five troughs instead of seven at an inlet temperature of 30°C and an 11 percent increase for five troughs instead of seven at an inlet temperature of 60°C. For an inlet temperature of 90°C, four troughs increased the useful energy by 58 percent. The main reason for the increases in useful energy at higher temperatures is that the concentration ratios are higher for a "flatter" parabola. The disadvantage for a "flatter" parabola is its poorer ability to concentrate off-normal radiation. The off-normal radiation, however, was minimized by optimizing the collector orientation first.

The distribution of losses for a five-trough collector with an absorber width of 30 mm and a bottom clearance of 10.2 mm is shown in Fig. 15. When Fig. 15 is compared to Fig. 5, a notable increase in efficiency results for the five-trough collector for temperature differences greater than 30°C. The "optical" losses are four percentage points higher for the five-trough collector because the "flatter" parabola is more sensitive to off-normal radiation, which results in larger beam intercept losses. The higher "optical" losses of the five-trough collector are offset as a result of increasing the concentration ratio by 40 percent over the previous design. With a higher concentration ratio, the overall loss coefficient is lower, which enables higher

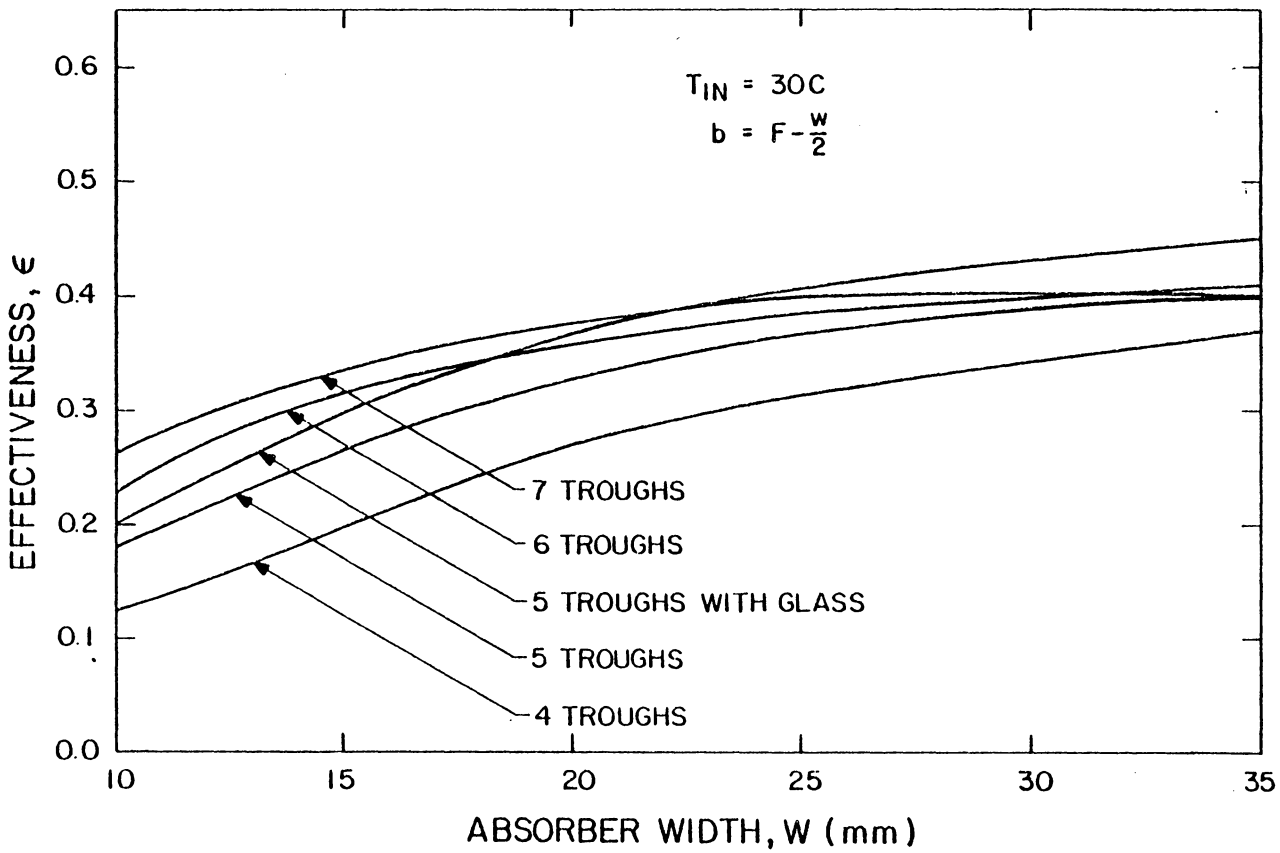

Figure 12. Optimum Number of Troughs and Absorber Widths for T_{IN} = 30°C

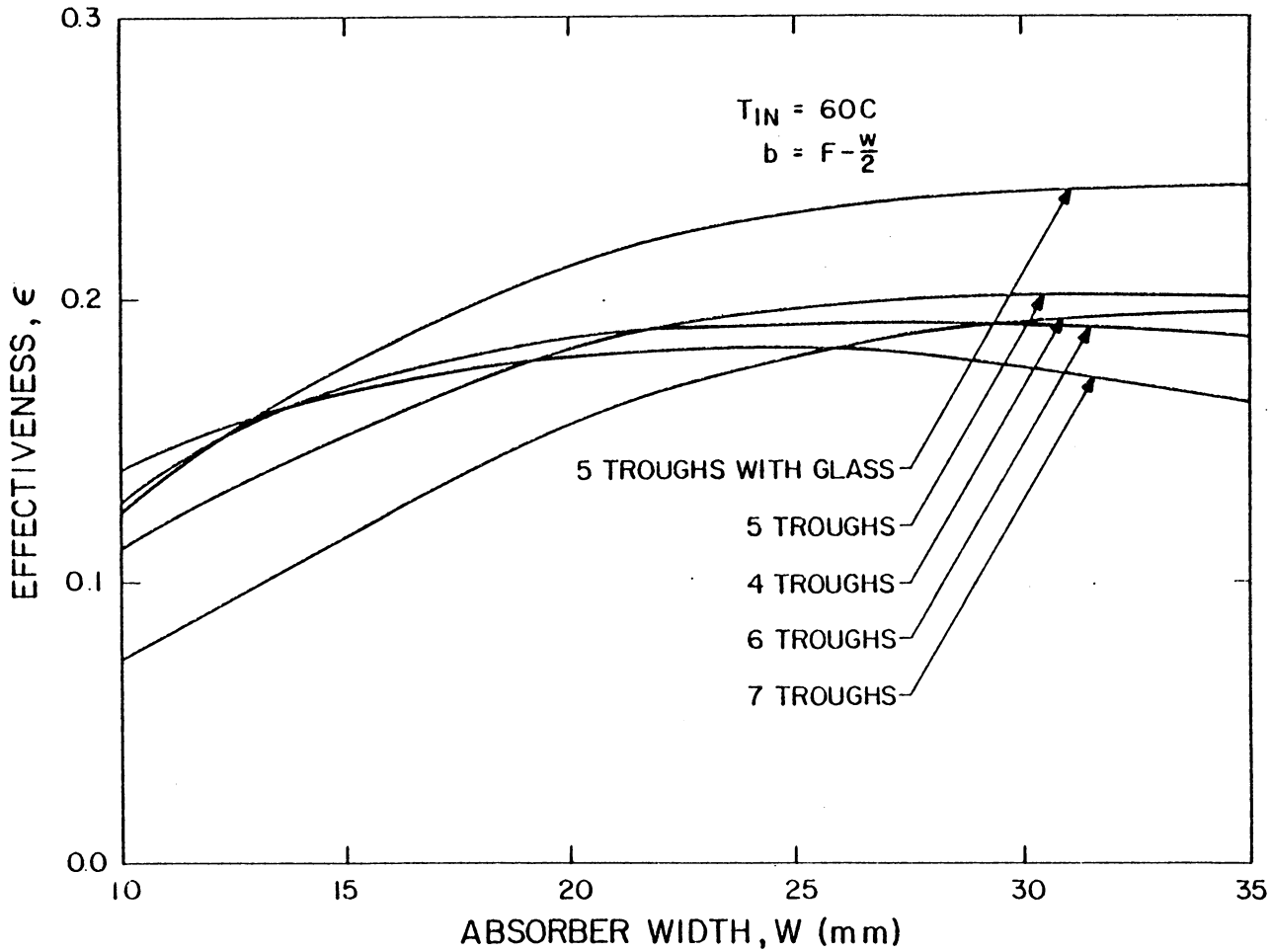

Figure 13. Optimum Number of Troughs and Absorber Widths for T_{IN} = 60°C

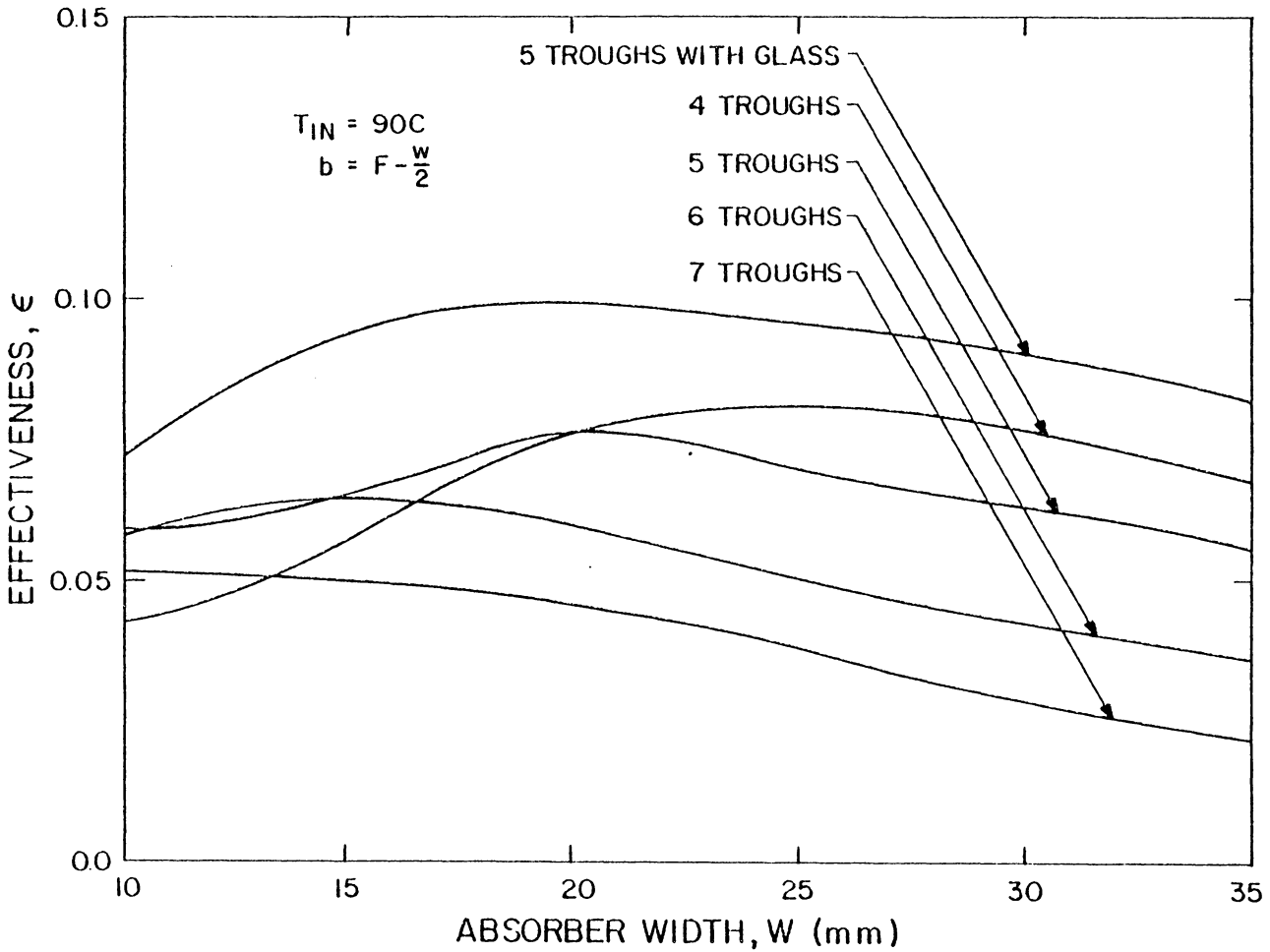

Figure 14. Optimum Number of Troughs and Absorber Widths for T_{IN} = 90°C

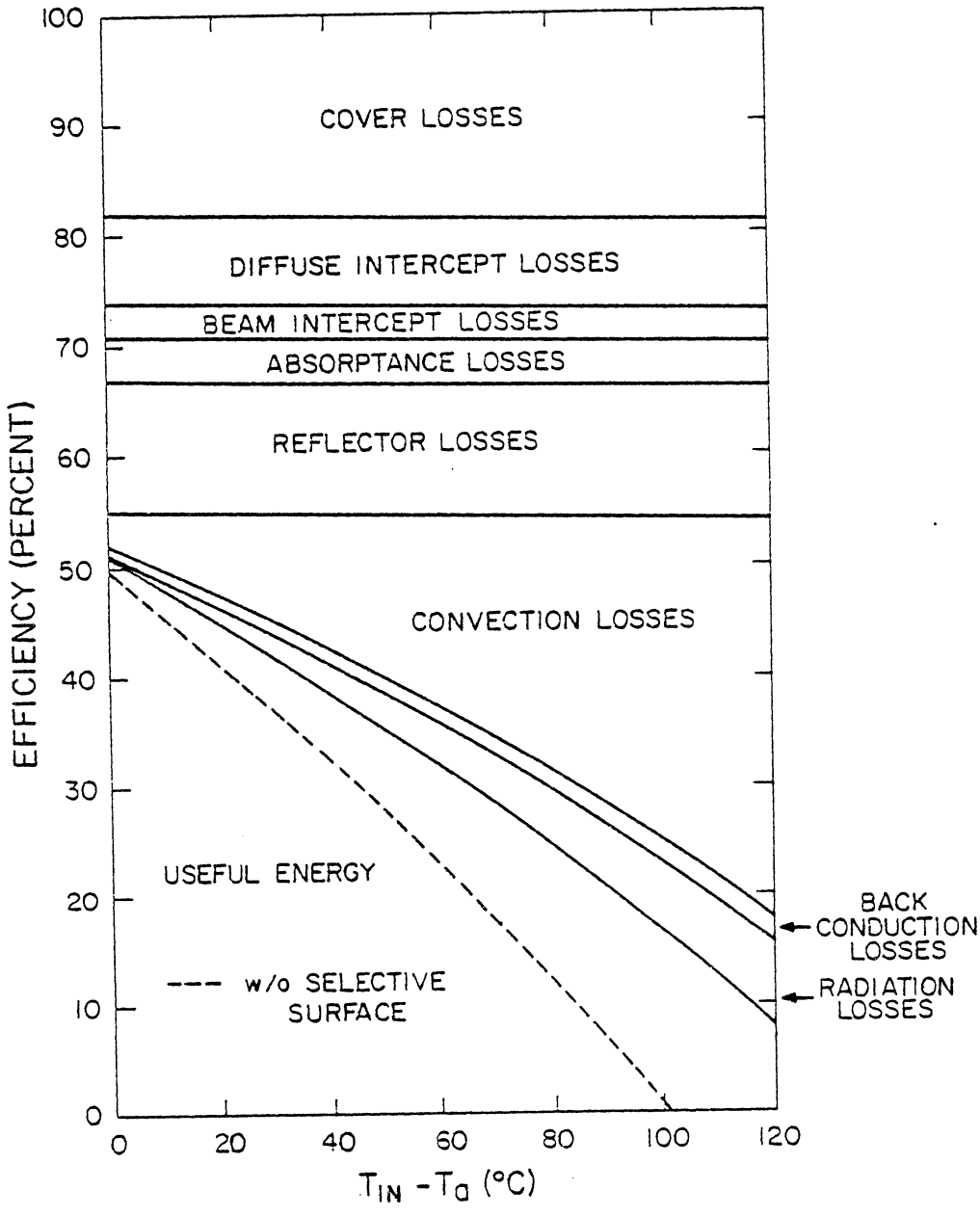

Figure 15. Distribution of Losses for the Optimum Dimensions of a Five-Trough Collector Using a Llumar Cover

efficiencies for high inlet temperatures.

Changing the cover material to glass and adding a Teflon tube around the absorber were also considered. The glass cover reduced the cover losses by 35 percent. Fig. 16 is similar to Fig. 15 but with a glass cover. Again, changing the cover to glass improved the efficiency by four percentage points for the entire range of temperature differences. Adding a Teflon tube over the absorber was difficult to analyze analytically; therefore, the performance was investigated experimentally. The experimental results showed that the Teflon tube caused a 2.5 percentage point decrease in efficiency for an inlet temperature equal to the ambient temperature. This value was close to the anticipated decrease in efficiency. The Teflon tube also caused a four percentage point decrease in efficiency for a temperature difference of 70°C, which was not expected. The Teflon tube should have suppressed the convection losses, which would decrease the overall loss coefficient and cause higher efficiencies at high inlet temperatures. The comparison was made with two similar collectors, one having Teflon tubes around the absorbers and the other in its original condition. The most likely explanation for the discrepancy at high inlet temperatures is that the modified collector could have been damaged in the process of adding the Teflon tubes. During the process of desoldering the absorber tubes in order to insert the Teflon tubes, a misalignment of the absorber tubes apparently resulted in optical losses and thermal shorts to the collector casing. Other possibilities that were considered but eliminated are degradation of the selective surface by the soldering process and small openings in the Teflon tubes.

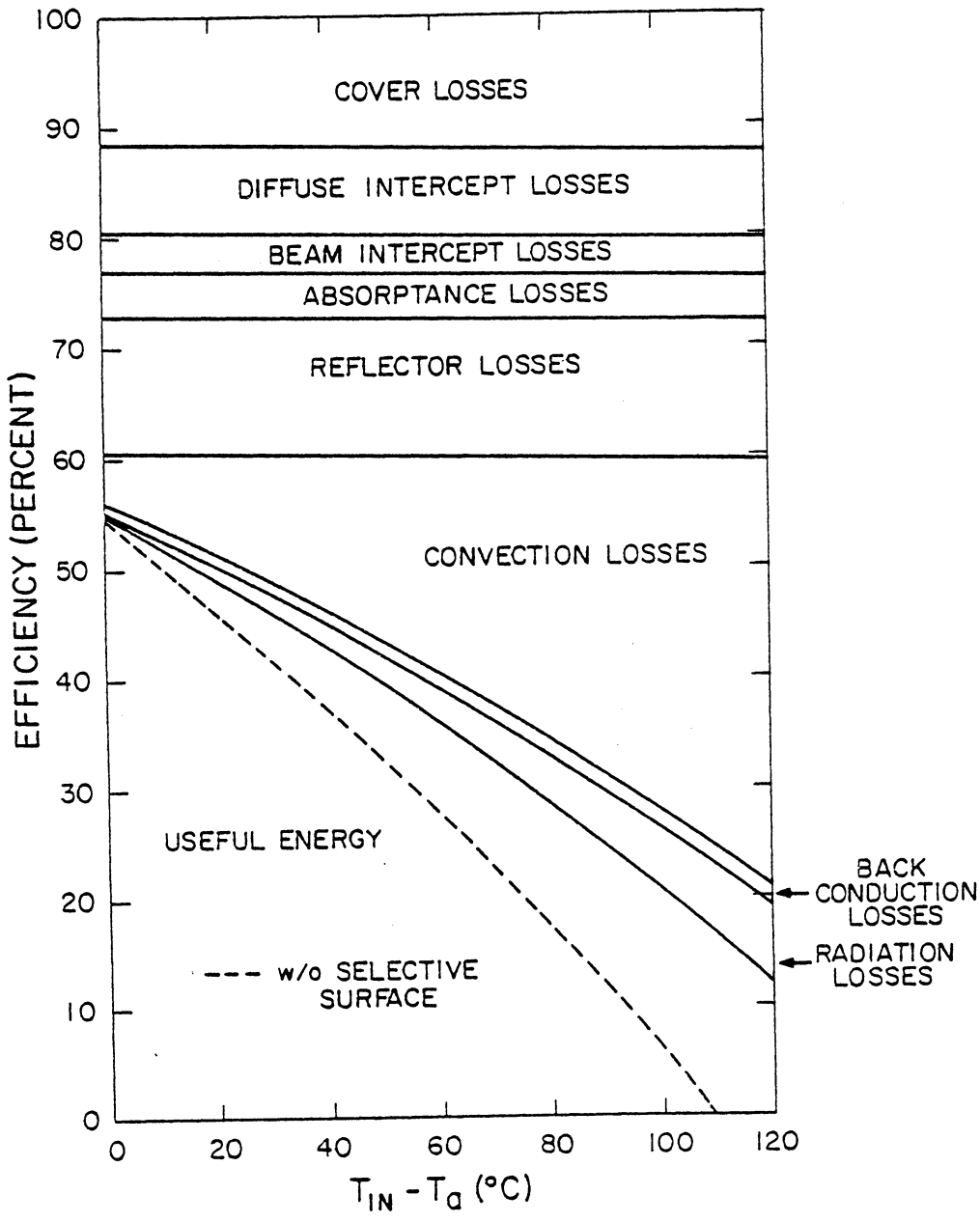

Figure 16. Distribution of Losses for the Optimum Dimensions of a Five-Trough Collector Using a Glass Cover

For a concentrating collector to be successful commercially, it must be able to compete against the conventional flat-plate collector. The distribution of losses for a typical flat-plate collector is shown in Fig. 17. The flat-plate collector has a single 3.2 mm-thick tempered glass cover with an absorber formed from two steel sheets which are stitch-welded and pressure expanded to form the flow passages. The absorber also has a selective surface and is backed by fiberglass insulation. Without the reflection and beam intercept losses of a concentrating collector, the "optical" efficiency of the flat-plate collector is approximately 84 percent. The overall loss coefficient, however, is higher than for a concentrating collector as a result of the large absorber area in a flat-plate collector. For temperature differences lower than 35°C, the flat-plate collector in Fig. 17 will out-perform the concentrating collector in Fig. 5, regardless of the thermal losses in the concentrating collector. The reason is that the "optical" efficiency of the concentrating collector in Fig. 5 is equal to the flat-plate efficiency at a temperature difference of 35°C. Unless the "optical" losses or manufacturing costs of concentrating collectors can be reduced, low temperature applications of solar energy will generally be restricted to flat-plate collectors.

The results of this optimization study are summarized in Fig. 18 and Table 3. The efficiency curves in Fig. 18 were obtained using the environmental and operating conditions in Table 2 and the collector designs previously discussed. The curves in Fig. 18 are instantaneous values for a clear day during the season, while the values in Table 3 are seasonal values. Fig. 18 shows that the flat-plate collector has a

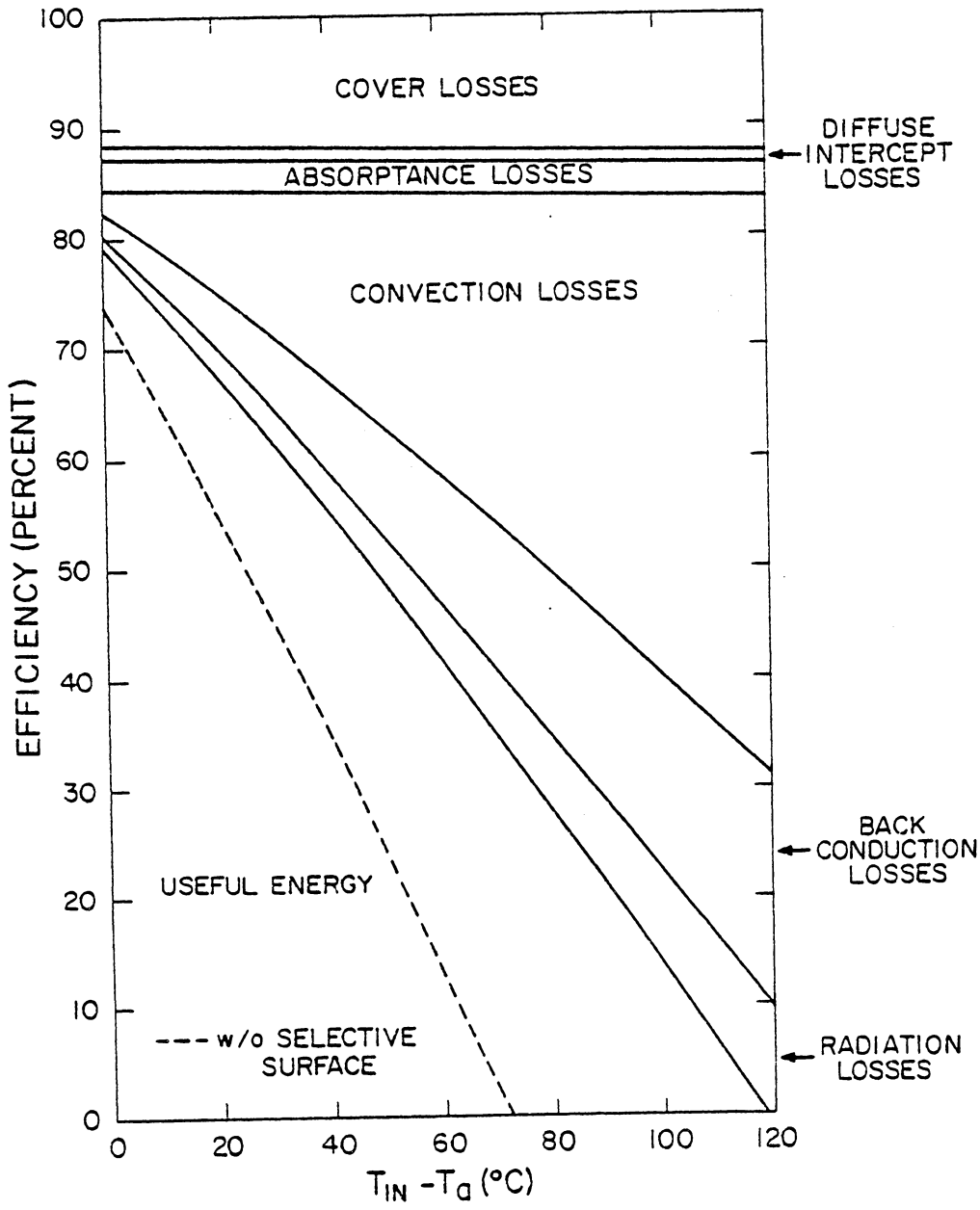

Figure 17. Distribution of Losses for a Flat-Plate Collector Using a Glass Cover

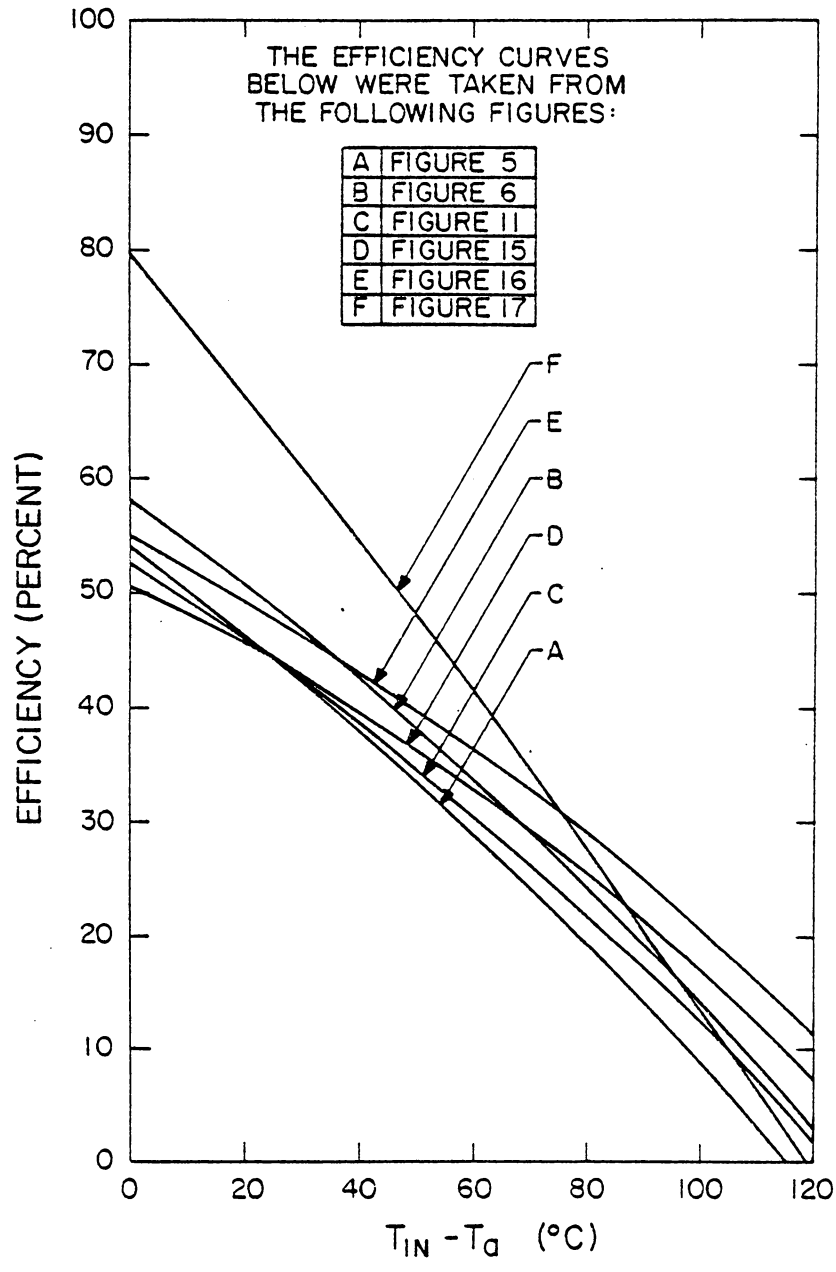

Figure 18. Comparison of Different Collector Designs

Table 3. COMPARISON OF COLLECTOR OPTIMIZATION RESULTS

COLLECTOR DESCRIPTION	T_{in} = 30C				T_{in} = 60C				T_{in} = 90C			
	W (mm)	b (mm)	W_a (mm)	ε	W (mm)	b (mm)	W_a (mm)	ε	W (mm)	b (mm)	W_a (mm)	ε
Present Design Llumar Cover 7 Troughs ρ_r=0.80, α_p=0.93 ε_p=0.20, τ_n=0.82	31.7	2.5	120	0.405	31.7	2.5	120	0.172	31.7	2.5	120	0.028
Optimum Design Llumar Cover 7 Troughs ρ_r=0.80, α_p=0.93 ε_p=0.20, τ_n=0.82	30.0	0.0	120	0.405	25.0	0.0	120	0.183	10.0	7.9	120	0.052
Optimum Design Llumar Cover 5 Troughs ρ_r=0.80, α_p=0.93 ε_p=0.20, τ_n=0.82	35.0	7.7	168	0.395	30.0	10.2	168	0.202	20.0	15.2	168	0.077
Optimum Design Glass Cover 5 Troughs ρ_r=0.80, α_p=0.93 ε_p=0.20, τ_n=0.89	35.0	7.7	168	0.449	30.0	10.2	168	0.240	20.0	15.2	168	0.099
Flat-Plate Collector Glass Cover α_p=0.96, ε_p=0.12 τ_n=0.89	--	--	--	0.763	--	--	--	0.342	--	--	--	0.065

higher efficiency than the best concentrating collector design for temperature differences less than 75°C. The more efficient collector, however, is not always the more economical collector and the cost per amount of energy collected should be considered.

After taking into consideration other collector designs, the cylindrical-parabolic collector is best suited for high temperature applications such as process heat. Based on the operating environment selected, the best thermal performance for process heating with the present general design and collector thickness is realized with four troughs and an absorber with a width of 25 mm located 27 mm above the bottom of the reflector. Fig. 14 shows that these optimum dimensions result in an effectiveness of 0.082 for an inlet temperature of 90°C. While it is possible to increase the effectiveness up to 0.103 by substituting a high quality glass for the existing cover, it is uncertain whether the added cost, extra weight and chance of breakage will justify the increase in effectiveness.

Although the cylindrical-parabolic collector is better suited for an inlet temperature of 90°C, the relatively low cost of conventional energy sources may make it difficult for the collector to compete on a purely economic basis in the near term future. The weather model shows that, on the average, approximately 510 kw-hr/m^2 of solar energy is incident on a horizontal surface in Blacksburg, Virginia, from October to March. A 2.0 m^2 collector having an effectiveness of 0.082 will collect 84 kw-hr from October to March at Blacksburg, Virginia. This amount of energy corresponds to a $2.52 present value worth of electrical energy (at $0.03 per kw-hr.). Therefore, a considerable escalation in energy

cost or an improvement in the collector effectiveness must occur before cylindrical-parabolic collectors are cost-competitive for process heat.

IV. CONCLUSIONS AND RECOMMENDATIONS

A seasonal performance model was used to investigate a cylindrical-parabolic solar collector. Without further improvements in collector materials, the optimum performance for the type of cylindrical-parabolic in this investigation was realized. The optimum dimensions and materials for a concentrating collector are a strong function of the design operating temperatures. For process heating, heat loss by natural convection is the major loss term. Reflection and cover losses are the next largest losses in a concentrating collector.

The optimum position of the absorber is centered at the focal point of the parabola. To take advantage of higher concentration ratios resulting from a "flatter" parabola, the collector orientation must be optimized. Substituting a high quality glass for the present cover could add approximately four percentage points to the efficiency for all inlet temperatures but would add cost, weight, and increase the breakage potential to the collector.

A flat-plate collector is more suited for domestic hot water and space heating while a concentrating collector appears more suited for process heat. Economics are important in determining the optimum design and the cost per amount of energy collected should be considered.

Since other concentrating collector designs have essentially the same components as the cylindrical-parabolic collector investigated in this study, the "optical" losses for other concentrating collector designs would be similar to that for the cylindrical-parabolic collector. Therefore, concentrating collectors with high concentration ratios and

large acceptance angles, such as the Winston compound parabolic collector, should give higher performances for the temperature ranges used in process heating. An investigation comparing the thermal performance of other concentrating collectors with high concentration ratios to that of cylindrical-parabolic collectors is needed.

REFERENCES

1. Duffie, J. A., and W. A. Beckman, Solar Energy Thermal Processes, Wiley, 1975.

2. Jordan, R. C., and B. Y. H. Liu, Applications of Solar Energy for Heating and Cooling of Buildings, ASHRAE GRP170, Ashrae Publication, 1977.

3. Beckman, W. A., S. A. Klien, and J. A. Duffie, Solar Heating Design by the f-Chart Method, Wiley, 1977.

4. Kays, J., Harnessing the Sun, New York, Morgan and Morgan, Publishers, 1975.

5. Liu, B. Y. H., and R. C. Jordan, "A Rational Procedure for Predicting the Long Term Average Performance of Flat-Plate Solar Energy Collectors," Solar Energy, Vol. 7, 1963, pp. 53-74.

6. Whiller, A., "Solar Radiation Graphs," Solar Energy, Vol. 9, 1965, p. 165.

7. Liu, B. Y. H., and R. C. Jordan, "The Interrelationship and Characteristic Distribution of Direct, Diffuse, and Total Solar Radiation," Solar Energy, Vol. 4, 1960, pp. 1-19.

8. Norris, D. J., "Solar Radiation on Inclined Surfaces," Solar Energy, Vol. 10, 1966, pp. 72-76.

9. Norris, D. J., "Correlation of Solar Radiation with Clouds," Solar Energy, Vol. 12, 1968, pp. 107-110.

10. Iqbal, M., "Estimation of the Monthly Average of the Diffuse Component of Total Insolation on Horizontal Surfaces," Solar Energy, Vol. 20, 1978, pp. 101-105.

11. Heywood, H., "The Computation of Solar Radiation Intensities, Parts I and II," Solar Energy, Vol. 9, 1965, pp. 223-225, Vol. 10, 1966, pp. 46-52.

12. Bruno, R., "A Correction Procedure for Separating Direct and Diffuse Insolation on a Horizontal Surface," Solar Energy, Vol. 20, 1978, pp. 97-100.

13. Reddy, S. J., "An Empirical Method for Estimating Sunshine from Total Cloud Amount," Solar Energy, Vol. 15, 1974, pp. 281-285.

14. Reddy, S. J., "An Empirical Method for Estimation of Total Solar Radiation," Solar Energy, Vol. 13, 1971, pp. 289-290.

15. Thomas, W. C., "Concentrating Collector Performance Code and Notes," Version CCT, Non-published computer code and notes, Blacksburg, Virginia, 1977.

16. Smith, S. A., "Evaluation of a Cylindrical-Elliptic Concentrating Solar Collector," Masters Thesis, Mechanical Engineering Department, VPI&SU, 1977.

17. Meinel, A. B., and M. P. Meinel, Applied Solar Energy, Addison-Wesley Pub. Co., 1976.

18. Winston, R., and H. Hinterburg, "Principles of Cylindrical Concentrators for Solar Energy," Solar Energy, Vol. 17, 1975, pp. 255-258.

19. Winston, R., "Principles of Solar Concentrators of a Novel Design," Solar Energy, Vol. 16, 1974, pp. 89-96.

20. Allen, J., N. Levity, A. Rabl, K. Reed, W. Schertz, and R. Winston, "Development of Parabolic Concentrators for Solar Thermal Applications?," ASME Paper, 76-WA/SOL-11, 1976.

21. Rabl, A., "Collector with Cusplike Compound Parabolic Concentrator and Selective Absorber," Sharing the Sun, Solar Technology in the Seventies, Vol. 2, Joint Conf. ASISES and SESC, Winnipeg, Canada, August 15-20, 1976.

22. Weinbelt, J. A., and N. Thatree, "Design and Experimental Evaluation of a V-Groove Solar Collector," ASME Paper 76-HT-53, 1976.

23. Troung, H. V., and J. Villanueva, "The Compound Trapezoidal Collector," Proc. of the 1977 Annual Mtg. - ASISES, Orlando, Florida, June 6-10, 1977, Vol. 2, Section 26-28, pp. 35-36.

24. Shapiro, M. M., "Non-Focusing Solar Concentrators of Easy Manufacture," Solar Energy, Vol. 19, 1977, pp. 211-213.

25. Hottel, H. C., and A. Whillier, "Evaluation of a Flat-Plate Solar Collector Performance," Transactions of the Conference on the Use of Solar Energy, The Scientific Basis, Vol. II, Part I, Section A., 1955, pp. 74-104.

26. Data of total radiation for Winnipeg, Canada, are obtained from Mr. D. M. Robertson, Regional Meteorologist, District Aviation Forecast Office, Winnipeg, Canada.

27. Ramsey, J. W., J. T. Borzoni, and T. H. Holland, "Development of Flat-Plate Solar Collectors for the Heating and Cooling of Buildings," NASA CR-134804 prepared by Honeywell, Inc., NTIS No. N75-264951, June, 1975, pp. 123-144.

28. Thomas, W. C., "Thermal Efficiency Test Procedures and Results for a Cylindrical Concentrating Collector," Solar Concentrating Collectors, Proceedings of the ERDA Conference on Concentrating Solar Collectors, Session 6, Georgia Institute of Technology, September 26-28, 1977.

APPENDIX I

BEAM RADIATION GEOMETRY

Fig. 19 shows the beam radiation angles relative to this investigation. Equations for the incident angle and zenith angle are from Duffie and Beckman [1] and are listed below:

$$\cos\theta = \sin\delta(\sin\phi\cos S - \cos\phi\sin S\cos\gamma) + \cos\delta(\cos\phi\cos S\cos\omega + \sin\phi\sin S\cos\gamma\cos\omega + \sin S\sin\gamma\sin\omega). \quad (I.1)$$

$$\cos\theta_Z = \sin\delta\sin\phi + \cos\delta\cos\phi\cos\omega. \quad (I.2)$$

Equations for ψ and ζ are from Thomas [28] and are listed below:

$$\psi = S - \arctan(\tan\theta_Z\cos\gamma_{sun}). \quad (I.3)$$

$$\zeta = \arctan(\tan\theta_Z\sin\gamma_{sun}\cos\psi). \quad (I.4)$$

where

$$\gamma_{sun} = \arcsin(\cos\delta\sin\omega/\sin\theta_Z). \quad (I.5)$$

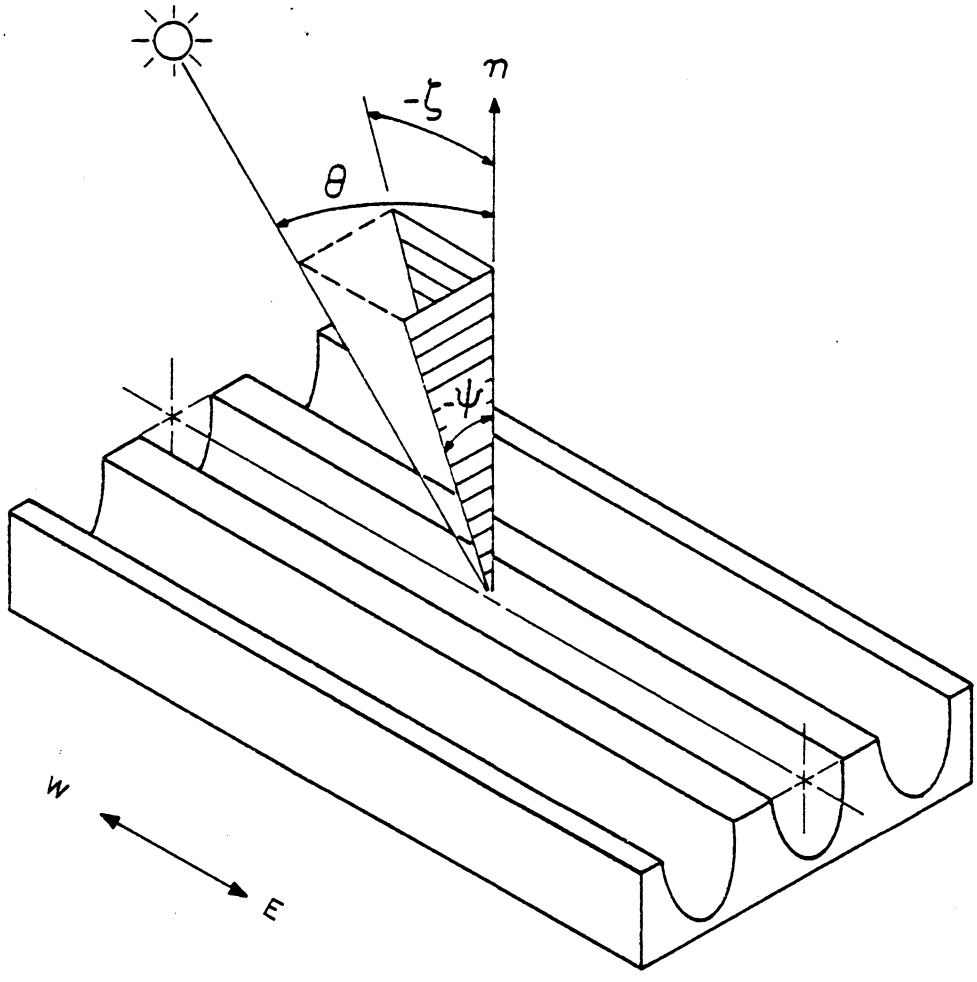

Figure 19. Collector Orientation and Beam Radiation Geometry

APPENDIX II

THERMAL PERFORMANCE MODEL

A thermal performance model is needed to calculate the useful energy collected, Q_u, and the efficiency, η_t, of a concentrating collector. A previous investigation [16] showed that the uneven flux distribution on the absorber can be treated as a mean flux because of the high thermal conductivity of the copper absorber. Basic collector modeling assumptions from Duffie and Beckman [1] are used along with the following additional assumptions:

1. The absorber is isothermal in the x-direction.
2. Axial conduction is negligible.
3. Steady-state conditions exist.
4. Scattered radiation is diffuse.

An energy balance is performed on the absorber which results in an equation comparable to the energy balance equation in [1], i.e.,

$$Q_u = 2WLF_R[S_m - U_L(T_{in}-T_a)], \tag{I.6}$$

where

$$F_R = \frac{GW_aC_p}{2WU_L}\left[1 - \exp\left(\frac{-2F'WU_L}{GW_aC_p}\right)\right], \tag{I.7}$$

$$F' = 1/\left(1 + \frac{2WU_L}{h_{f,i}W_p}\right), \tag{I.8}$$

$$h_{f,i} = Nu_{f,i}(K_f/D_e), \tag{I.9}$$

and

$$Nu_{f,i} = 3.66 + 0.0668(RePrD_e/L)/[1 + 0.04(RePrD_e/L)^{2/3}]. \tag{I.10}$$

The expression for Q_u involves the considerable tasks of evaluating the

mean solar flux incident on the absorber, S_m, and the overall loss coefficient, U_L. The mean solar flux on the absorber is composed of direct (non-reflected) beam radiation, reflected beam radiation, and scattered radiation in the trough.

$$S_m = 0.5(S_{B,L} + S_{B,R} + S_{r,L} + S_{r,R} + S_{D,L} + S_{D,R}), \tag{I.11}$$

where

$$S_{B,L} = \alpha_p \tau_B H_B \cos \zeta [\sin |\psi| + (\delta_t/W) \cos \psi], \tag{I.12}$$

$$S_{B,R} = 0, \tag{I.13}$$

$$S_{r,L} = \gamma_L H_B \cos \zeta, \tag{I.14}$$

$$S_{r,R} = \gamma_R H_B \cos \zeta, \tag{I.15}$$

$$S_{D,L} = \alpha_p (F_{pc}\hat{J}_c + F_{pr}\hat{J}_r), \tag{I.16}$$

and

$$S_{D,R} = \alpha_p (F_{pc}\hat{J}_c + F_{pr}\hat{J}_r). \tag{I.17}$$

The parameters γ_L and γ_R are the fractions of beam radiation incident on the collector which reaches the absorber by reflection for the left and right side. Fig. 20 shows two representa tive rays incident upon the reflector. For $\psi > 0$, Z_{min} is the greater of $\delta_t/2$ and the solution of

$$\frac{Z_{min} - \delta_t/2}{[W+b] - C(Z_{min})} = \tan \psi, \tag{I.18}$$

where $C(Z_{min})$ is the profile function evaluated at Z_{min}. For $\psi < 0$, Z_{min} is the greater of zero and $\delta_t/2 - b \tan \psi$. For $\psi > 0$, Z_{max} is $W_a/2$. For $\psi < 0$, Z_{max} is $W_a/2$ when

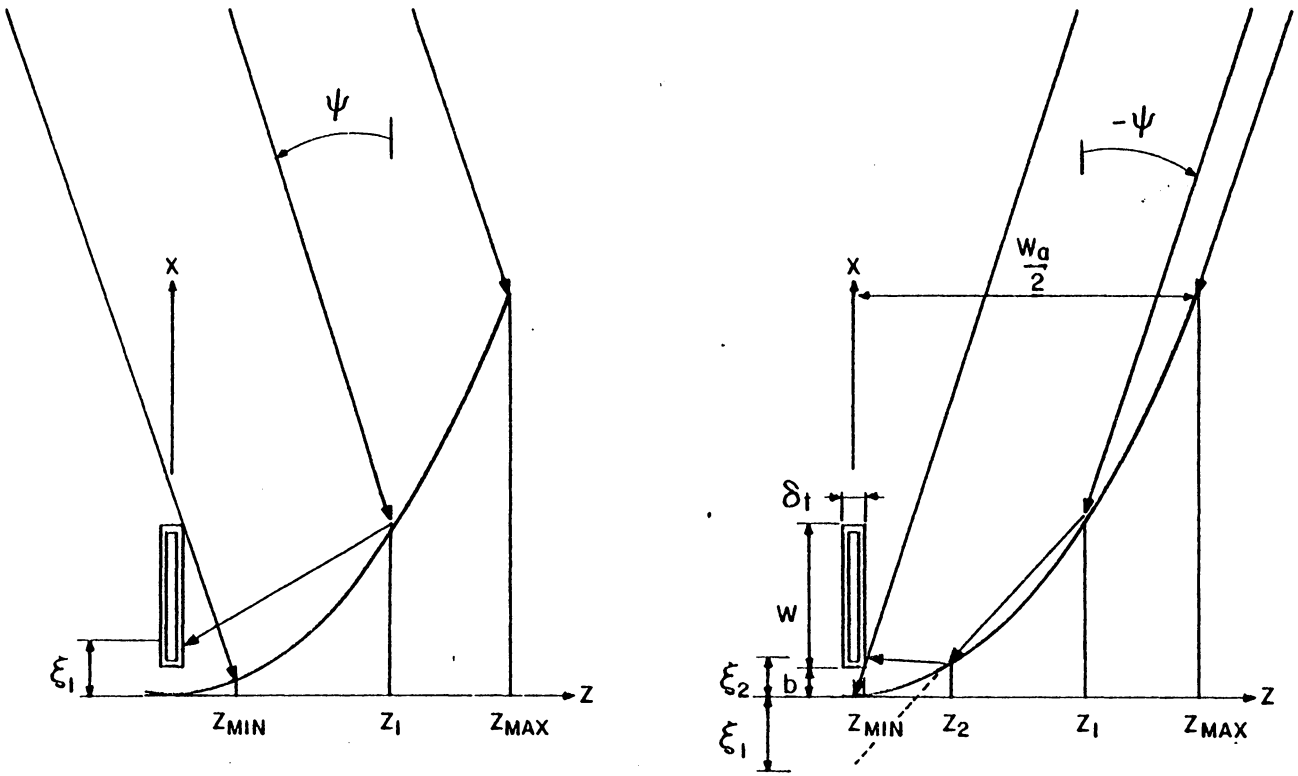

Figure 20. Ray-Trace Diagram for Off-Normal Ray Paths

$$\frac{dC(W_a/2)}{dZ} \leq \tan(\pi/2 + \psi), \tag{I.19}$$

and Z_{max} is the solution of

$$C(Z_{max}) = \left[Z_{max} - W_a/2\right] \tan(\pi/2 + \psi) + C(W_a/2) \tag{I.20}$$

when

$$\frac{dC(W_a/2)}{dZ} > \tan(\pi/2 + \psi). \tag{I.21}$$

The x-axis intercept of the reflected ray is

$$\xi(Z) = \frac{[1 - (dC/dZ)^2](Z - x \tan \psi) + 2(dC/dZ)(x + Z \tan \psi)}{2(dC/dZ) - [1 - (dC/dZ)^2] \tan \psi} \tag{I.22}$$

The ray hits the absorber if $b \leq \xi \leq (W + b)$. The ray is treated as diffuse if $0 \leq \xi < b$ or $\xi > (W + b)$. Multiple reflections occur if $\xi < 0$. If multiple reflections occur, the equation of the once-reflected ray is

$$X(Z) = [C(Z_1) - \xi_1] Z/Z_1 + \xi_1. \tag{I.23}$$

The second reflection occurs at Z_2, where Z_2 is found by solving

$$C(Z_2) = [C(Z_1) - \xi_1] Z_2/Z_1 + \xi_1. \tag{I.24}$$

The procedure is repeated for the once-reflected ray to find if a third or more reflections occur. If, after 11 reflections, ξ is still less than zero, the radiation associated with the ray is taken as an addition to the diffuse radiation component. For less than 11 reflections, the beam fraction reaching the absorber, for an increment ΔZ, is

$$\gamma_i = [\tau_B (\rho_B)^j \Delta Z \cos \psi]/W, \tag{I.25}$$

where j is the number of reflections. The total fraction of radiation reaching the absorber is

$$\gamma = \sum_{i=1}^{n} \gamma_i, \tag{I.26}$$

where

$$n = (Z_{max} - Z_{min})/\Delta Z. \tag{I.27}$$

The right side is evaluated with a positive ψ and the left side with a negative ψ. The process is repeated with ΔZ one-tenth as large to see if γ changes more than five percent. If so, ΔZ is repeatedly divided by 10 until the change is less than five percent.

The radiosities, $\hat{J}_c$ and $\hat{J}_r$, are obtained from a short wave radiation network analysis of the four surfaces shown in Fig. 21. The "imaginary" surface is introduced as a result of trough symmetry and is adiabatic, i.e., $\rho_i = 1$. The resulting equations for each surface are as follows:

Absorber:

$$-(1-\alpha_p)F_{pc}\hat{J}_c + (0)\hat{J}_i + \hat{J}_p - (1-\alpha_p)F_{pr}\hat{J}_r = (1-\alpha_p)(S_{r,L}+S_{r,R})/(2\alpha_p). \tag{I.28}$$

Cover:

$$\hat{J}_c - \rho_d F_{ci}\hat{J}_i - \rho_d F_{cp}\hat{J}_p - \rho_d F_{cr}\hat{J}_r = \tau_d H_D. \tag{I.29}$$

Imaginary surface:

$$-F_{ic}\hat{J}_c + J_i + (0)\hat{J}_p - F_{ir}\hat{J}_r = 0. \tag{I.30}$$

Reflector:

$$-\rho_r F_{rc}\hat{J}_c - \rho_r F_{ri}\hat{J}_i - \rho_r F_{rp}\hat{J}_p + (1-\rho_r F_{rr})\hat{J}_r =$$

$$H_B \cos\theta \tau_c (\rho_r)^r (Z_{max}-Z_{min})/W_r - (S_{r,L}+S_{r,R})W/(2W_r\alpha_p). \tag{I.31}$$

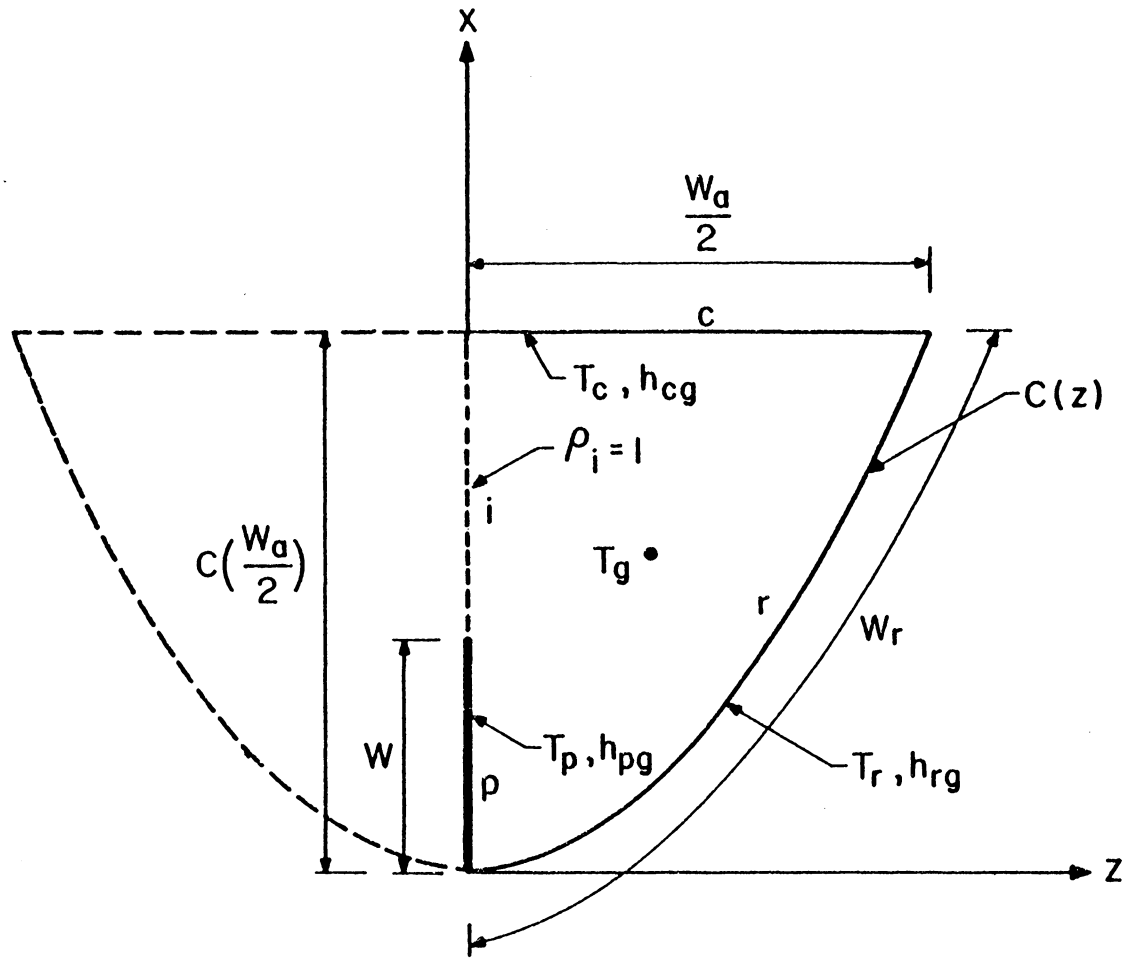

Figure 21. Collector Surfaces for Radiant Interchange

The previous four equations and four unknowns ($\hat{J}_c$, $\hat{J}_i$, $\hat{J}_p$ and $\hat{J}_r$) are solved by an iterative procedure.

The overall loss coefficient, U_L, is

$$U_L = \dot{q}_{loss}/[2W(T_p-T_a)] = [h_{pg}(T_p-T_g) + \varepsilon_p(\sigma T_p^4-J_p)/(1-\varepsilon_p)](1+\delta_t/W)/(T_p-T_a). \quad (I.32)$$

The mean absorber temperature, T_p, is treated as a known quantity for the rest of the analysis. The mean fluid temperature, T_f, will later be calculated and used to recalculate the mean absorber temperature, and the entire calculation procedure repeated until convergence occurs. The absorber long wave radiosity, J_p, is found by solving a system of equations containing the radiosity of each surface in terms of the surface temperature, configuration factors, and surface properties. The four equations which result are:

Cover:

$$J_c - \rho_c F_{ci} J_i - \rho_c F_{cp} J_p - \rho_c F_{cr} J_r = \varepsilon_c E_{bc} + \tau_c E_{bs}. \quad (I.33)$$

Imaginary surface:

$$-F_{ic} J_c + J_i + (0)J_p - F_{ir} J_r = 0. \quad (I.34)$$

Absorber:

$$-\rho_p F_{pc} J_c + (0)J_i + J_p - \rho_p F_{pr} J_r = \varepsilon_p E_{bp}. \quad (I.35)$$

Reflector:

$$-\rho_r F_{rc} J_c - \rho_r F_{ri} J_i - \rho_r F_{rp} J_p + (1-\rho_r F_{rr})J_r = \varepsilon_r E_{br}. \quad (I.36)$$

It should be noted that the surface optical properties used in Eqs.

(I.33)-(I.36) are long wave values.

The temperatures of the cover, gas and reflector are found by energy balances on the collector components. The equations for the energy balances are:

Gas:

$$-W_a h_{cg} T_c/2 + (Wh_{pg}+W_r h_{rg}+W_a h_{cg}/2)T_g - W_r h_{rg} T_r = Wh_{pg} T_p. \qquad (I.37)$$

Reflector:

$$(0)T_c - h_{rg} T_g + (\varepsilon_r \sigma T_r^3/\rho_r + h_{rg} + K_r/L_r)T_r = \varepsilon_r J_r/\rho_r + K_r T_a/L_r + \dot{Q}_{rad}, \qquad (I.38)$$

where $\dot{Q}_{rad}$ is the short wave beam and diffuse radiation absorbed by the reflector.

Cover:

$$(2\varepsilon_c \sigma T_c + h_w + h_{cg})T_c - h_{cg} T_g + (0)T_r =$$

$$\alpha_{Bc} H_B \cos\theta + h_w T_a + \alpha_{Dc}[H_D + \hat{G}_c] + \alpha_c [E_{bs} + G_c]. \qquad (I.39)$$

The mean solar flux on the absorber and the overall loss coefficient can now be calculated. With these values, the useful energy collected can be calculated by Eq. (I.6). The mean fluid temperature, T_f, is

$$T_f = T_{in} + Q_u(1-F_R/F')/(2WLU_L F_R). \qquad (I.40)$$

The mean fluid temperature is used to recalculate the mean plate temperature, which is

$$T_p = T_f + Q_u/(h_{fi} W_p L). \qquad (I.41)$$

The calculation procedure is repeated until the recalculated and trial

plate temperatures converge. After convergence, the efficiency can be calculated as

$$\eta = Q_u/(H_T^t A_C). \tag{I.42}$$

The vita has been removed from the scanned document

ANALYSIS AND DESIGN OF A CYLINDRICAL PARABOLIC SOLAR COLLECTOR

by

Aaron Grayson Dawson, III

(ABSTRACT)

A cylindrical-parabolic solar collector was thermally optimized for a winter season using a weather model and an extension of the present state-of-the-art collector theory. An accurate model for the cover transmittance and a seasonal performance model was developed. The optimum collector dimensions and materials were found to be a strong function of the design operating temperatures. The optical and thermal losses of a cylindrical-parabolic collector were compared and the results showed that the major loss for process heating temperatures was heat lost by natural convection. Reflection and cover losses were the next largest losses. Comparison of a flat-plate collector with a cylindrical-parabolic collector showed that a cylindrical-parabolic collector appears better suited for process heating than domestic hot water or space heating. Glass and plastic covers were analyzed and the optimum collector slope was obtained. The investigation resulted in a better understanding of how different collector dimensions and materials affect collector performance.